iScience

CellPress
OPEN ACCESS

Article

Low Shear Stress Increases Recombinant Protein Production and High Shear Stress Increases Apoptosis in Human Cells

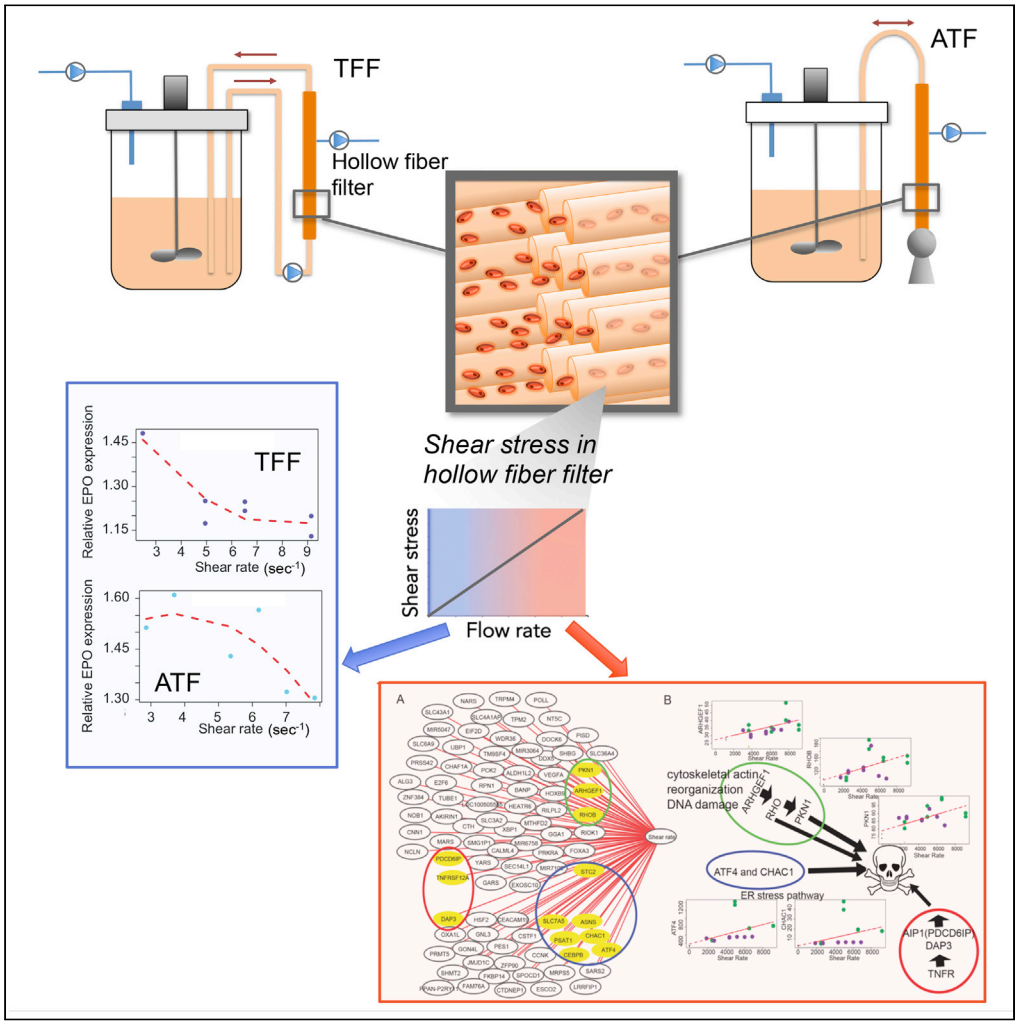

Caijuan Zhan, Gholamreza Bidkhori, Hubert Schwarz, ..., Adil Mardinoglu, Johan Rockberg, Veronique Chotteau

chotteau@kth.se

HIGHLIGHTS

Fluid dynamics, transcriptomics, and phenotype study to understand the perfusion impact

Mild shear stress has favorable effects on protein transcription and phosphorylation

High shear stress provokes apoptosis by three different pathways

Average shear rate in hollow filter cell separation device ATF is lower than in TFF

Zhan et al., iScience 23, 101653
November 20, 2020
https://doi.org/10.1016/j.isci.2020.101653

iScience

CellPress
OPEN ACCESS

Article

Low Shear Stress Increases Recombinant Protein Production and High Shear Stress Increases Apoptosis in Human Cells

Caijuan Zhan,[1,5,6,7] Gholamreza Bidkhori,[2,7] Hubert Schwarz,[1,5,6] Magdalena Malm,[3,5] Aman Mebrahtu,[3,5] Ray Field,[4] Christopher Sellick,[4,8] Diane Hatton,[4] Paul Varley,[4,8] Adil Mardinoglu,[2] Johan Rockberg,[3,5,6] and Veronique Chotteau[1,5,6,9,*]

SUMMARY

Human embryonic kidney cells HEK293 can be used for the production of therapeutic glycoproteins requiring human post-translational modifications. High cell density perfusion processes are advantageous for such production but are challenging due to the shear sensitivity of HEK293 cells. To understand the impact of hollow filter cell separation devices, cells were cultured in bioreactors operated with tangential flow filtration (TFF) or alternating tangential flow filtration (ATF) at various flow rates. The average theoretical velocity profile in these devices showed a lower shear stress for ATF by a factor 0.637 compared to TFF. This was experimentally validated and, furthermore, transcriptomic evaluation provided insights into the underlying cellular processes. High shear caused cellular stress leading to apoptosis by three pathways, i.e. endoplasmic reticulum stress, cytoskeleton reorganization, and extrinsic signaling pathways. Positive effects of mild shear stress were observed, with increased recombinant erythropoietin production and increased gene expression associated with transcription and protein phosphorylation.

INTRODUCTION

Operating a bioreactor in perfusion mode allows for a continuous renewal of the culture medium, generating a stable and favorable environment in the bioreactor, which can benefit the cell metabolism and growth but even more importantly allows higher volumetric yield and product quality (Chotteau, 2015; Gomez et al., 2019). This has recently awakened an increasing interest in the biopharmaceutical field. Perfusion processes require smaller bioreactors and reduced footprint compared to batch or fed-batch processes, leading to lower capital expenditure. Numerous continuous processes for mammalian cell cultures have been reported for manufacture of products such as monoclonal antibodies, glycoproteins and baculovirus (Takamatsu et al., 1996; Wang et al., 2002; Zhu, 2012; Merten et al., 1999).

A suitable cell retention device is critical for operating a successful perfusion process. Several cell separation techniques are industrially used for perfusion operations, e.g. gravity-based cell settler, spin filters, centrifuge, tangential flow filtration (TFF) and alternating tangential flow filtration (ATF), as reviewed in previous reports (Castilho and Medronho, 2002; Voisard et al., 2003; Woodside et al., 1998). TFF can minimize the filter fouling since the particles are not pressed into the filter membrane. Among these systems, hollow fiber filter (HF)-based cell separation is efficient and has shown to support very high cell density for biopharmaceutical manufacturing (Gálvez et al., 2012; Clincke et al., 2013a, 2013b). Introduced by Shevitz (Shevitz, 2000), alternating TFF can further reduce the filter fouling by creating a back flush in the filter membrane. In the ATF, the cell suspension is pumped from the bioreactor to the HF and *vice versa* thanks to a diaphragm pump mounted at one end of the HF, while the cell suspension is circulated only in one direction in the TFF using a peristaltic pump.

Many mammalian cells are sensitive to shear or mechanical force, and various studies have shown that high levels of shear can affect the cell viability and growth (Garcia-Briones and Chalmers, 1994; Gregoriades et al., 2000). Ideally, to achieve high cell density while maintaining a high productivity, the cells should

[1]KTH - Cell Technology Group (CETEG), Department of Industrial Biotechnology, 106 91, Stockholm, Sweden

[2]Science for Life Laboratory, KTH - Royal Institute of Technology, 171 21, Stockholm, Sweden

[3]KTH - Royal Institute of Technology, Department of Protein Science, 106 91 Stockholm, Sweden

[4]BioPharmaceutical Development, AstraZeneca, Cambridge, UK

[5]Wallenberg Centre for Protein Research (WCPR), 106 91 Stockholm, Sweden

[6]AdBIOPRO, Competence Centre for Advanced Bioproduction by Continuous Processing, Stockholm, Sweden

[7]These authors contributed equally

[8]Formerly at AstraZeneca

[9]Lead Contact

*Correspondence: chotteau@kth.se

https://doi.org/10.1016/j.isci.2020.101653

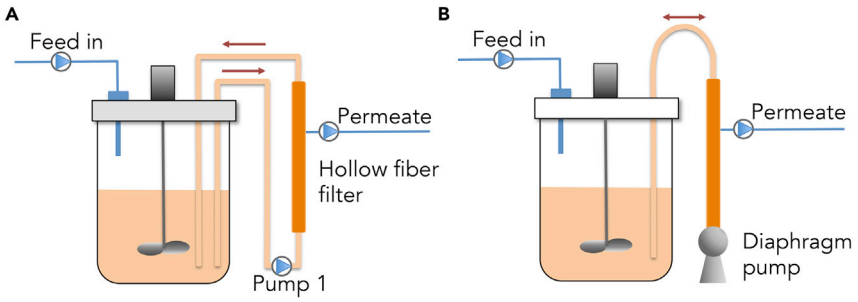

Figure 1. Overview of a Bioreactor Connected to Hollow Fiber Filter Cell Separation for Perfusion Process by TFF or ATF

Schematic diagram of (A) tangential flow filtration, TFF, where pump 1 was an Alitea XV pump with a flow rate of up to 0.19 L/min, or two Alitea XV pumps mounted in parallel for 0.38 L/min, or the diaphragm pump of an ATF2 mounted with two one-way valves for flow rates >0.38 L/min; (B) alternating tangential flow filtration, ATF.

not be submitted to significant shear or mechanical damage. Therefore, the operation parameters should be carefully chosen such that the hydrodynamic conditions do not significantly damage the cells. In the HF-based perfusion culture setting, there are two main locations where shear cell damage occurs: the bioreactor and the cell separation device. In the bioreactor, the aeration and associated foam and bubble formations can be detrimental, as well as the agitation generated by the impeller(s) for culture homogenization. The energy dissipation rate (EDR) accounts for all potential types of fluid stress and is commonly used to characterize the fluid flow and characterize the hydrodynamic conditions that can damage the cells in bioprocesses of established cells. Chalmers and Ma (Chalmers and Ma, 2015) studied the EDR generated from different sources in the bioreactor and identified non-lethal and lethal effects on the cells. The EDR and shear stress are related in a way specific to the source of the shear damage. Concerning the cell separation device, shear is created by the passage of the cells in the hollow fiber lumens. The flow in a hollow fiber lumen can be characterized as Poiseuille flow for Newtonian fluids.

Whilst Chinese Hamster Ovary (CHO) cells are the workhorse of the biopharmaceutical industry, alternative cells of human origin such as HEK293 cells can provide recombinant glycoproteins with human post-translational modifications that are of critical importance for certain therapeutic indications. For instance, HEK293 cells have been recently adopted for the production of several recombinant factors of the blood coagulation cascade such as factor VIII but also commercially explored for the production of erythropoietin or enzymes (Kumar, 2015; Lalonde and Durocher, 2017; Llop et al., 2008; Swiech et al., 2012).

The purpose of the present study was to understand how the shear stress generated by a HF used for cell separation by TFF or ATF could impact HEK293 cells. We studied theoretically the velocity profile and shear stress for these two filtration systems. To support these results, we studied the sensitivity of a HEK293 cell line producing recombinant human erythropoietin (rhEPO) to hydrodynamic forces in parallel batch experiments using mini bioreactors system equipped with TFF or ATF at different flow rates. This phenotypic study was complemented by a systematic investigation of the global functional response of HEK293 cells to shear stress by transcriptomics. We introduced a functional map of the impact of shear stress on the HEK293 cells, manifested in cellular functions including immune and inflammatory responses, oxidative stress, cytoskeleton reorganization, endoplasmic reticulum (ER) stress, apoptosis, and cell cycle. This study provides a detailed experimental and theoretical study to understand the shear stress effects on HEK293 cells occurring in TFF and ATF systems during perfusion operation.

RESULTS

Theoretical Considerations - Shear Stress Characterization

Shear stress develops when a liquid is in motion due the relative movement of fluid particles with each other. The shear stress, which is the force exerted on the cells in a culture, is due to the velocity gradient and not directly to the flow rate itself. Thus the same flow rate can lead to different levels of shear stress. In a laminar flow, the shear rate is the velocity gradient and the shear stress is equal to the shear rate times the viscosity. The TFF and ATF systems were described in the Introduction and a schematic representation is given in Figure 1. In a TFF, the re-circulation fluid velocity is constant while in an ATF it has a sinusoidal

profile varying between a maximum value and zero (Figure S1), due to flow in alternating directions. Consequently, for a given re-circulation flow rate, the shear rate in the HF of a TFF, γ_{TFF}, is constant while it is varying in an ATF. The maximal absolute value of the shear rate in the ATF is equal to γ_{TFF} and achieved twice per cycle but the instantaneous absolute shear rate is lower most of the time. In the range 0 to π, the average absolute shear rate in the ATF, γ_{ATF}, can be expressed as a function of its maximum absolute value (equal to γ_{TFF}), as follows:

$$\gamma_{ATF} = \frac{\partial U_0}{\partial y} \frac{\int_0^{\pi} \sin(\omega t) \cdot d\omega t}{\pi} = \gamma_{TTF} \frac{2}{\pi} \approx 0.637 \gamma_{TFF} \qquad \text{(Equation 1)}$$

where u is the velocity of the fluid (m/s), $\partial U_0/\partial y = \gamma_{TFF}$ is the constant shear rate occurring in the TFF, ω is the frequency of the ATF cycle (s^{-1}) calculated from the flow rate of the ATF, t is time. Detailed calculations are given in Supplemental Information - Transparent Methods - Section A.1.

This result implies that the average absolute shear rate is lower in the ATF than in the TFF and is $2/\pi \approx 0.637$ of the shear rate in the TFF, although the instantaneous shear rate in the ATF system has a maximum equal to the constant shear rate in the TFF system. So, the average absolute shear stress in the ATF, $\tau_{ATF} = \tau_{TFF}\, 2/\pi \approx 0.637\, \tau_{TFF}$. For instance, for a flow rate of 1 L/min, the shear stress in the ATF and the TFF are 8.3 and 13 N/m^2, respectively, (applying S.3 and S.4).

Shear Stress Effect on Cell Growth

To experimentally confirm the results obtained from the theoretical exercise of "Section Theoretical considerations - Shear stress characterization", parallel batch cultivations were performed with cells subjected to the ATF or the TFF systems, see Figure 1. As a control in an attempt to remove the effect of the pumps and to consider only the shear stress effect from the passage in the hollow fibers of the TFF independently of the pump, a preliminary investigation was performed to characterize a system where pumping did not affect the cells. For this, the bioreactors were equipped with a system similar to the TFF perfusion culture where the HF cartridge was shortcut, i.e. removed. With this system, the effect of cell damage at a flow rate of 0.3 L/min, operated by a peristaltic pump, was studied in 5-day batch mode using two different pump tubing's of the same diameter: GORE STA-PURE and PharMed. It was observed that the PharMed pump tube led to low cell viability and poor growth after one day of culture as shown in Figure 2A. Isn contrast, the cell culture using GORE STA-PURE pump tube had a high growth rate and viability. The GORE STA-PURE has a smooth inner wall in Teflon while the PharMed has a rough inner surface deteriorating the cells during the pumping in the peristaltic pump. In all the subsequent experiments, the GORE STA-PURE tube was systematically used in the peristaltic pump of the TFF system.

The effect of the shear stress occurring in the hollow fiber cartridge in ATF and TFF systems was studied for different flow rates in 5-day batch culture as described in Transparent Methods. The operating conditions for ATF were 0.2–1 L/min (shear stress: 1.6–7.5 N/m^2) and for TFF were 0.127–0.7 L/min (shear stress 1.6–9.1 N/m^2), with absence of re-circulation 'No shear' as control condition.

The viable cell density and viability observed with different ATF or TFF flow rates are exemplified in Figures 2B and 2C. In both systems, there was no significant effect on the cell viability when the cells were re-circulated in these systems at the lowest flow rates, corresponding to the lowest shear stress. The cell viability decreased with time in the case of the high flow rates indicating that high flow rates and thus high shear rates led to cell death. The cell growth rate as function of increasing flow rate or shear stress using ATF and TFF systems is represented in Figure 2D-left and 2D-right. It can be seen that the growth rates using the TFF system clearly decreased with increasing flow rates for values $\geq$0.38 L/min. In the case of the ATF system, a similar decrease was mainly observed from flow rates $\geq$0.7 L/min Figure 2D-right represents the growth rate as a function of the average shear rate γ. This provides an indication of the effect of the shear rate on the cell growth or of the shear stress τ, which is directly proportional to the shear rate (Equation S3). Considering the average shear rate, which is theoretically lower by a factor 0.637 in the ATF system compared to the TFF, it was observed in Figure 2D-right that for shear rates larger than 4900 s^{-1} defined here as $\gamma_{threshold}$, or shear stress larger than 5 N/m^2, defined here as $\tau_{threshold}$, the growth rate was significantly lower, independently of the system, ATF or TFF (p value 0.0145). Polynomial regression analysis also predicted that the growth rate ratio (growth rate ratio = growth rate/control growth rate, where control is absence of flow 'No shear') is strongly associated with shear stress especially in TFF (adj $R^2 > 0.57$,

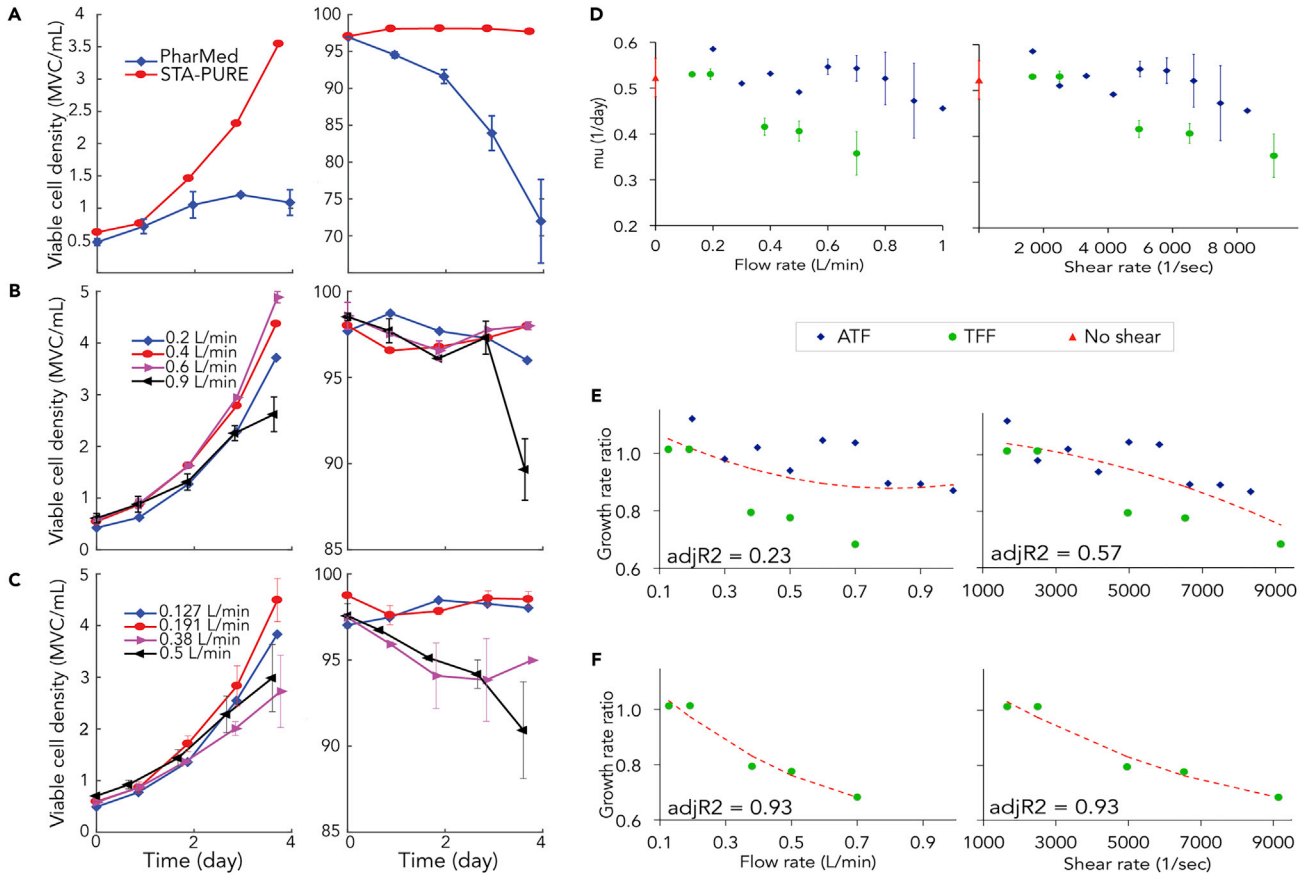

Figure 2. Effect of the Flow Rate and the Shear Rate on the Cell Growth and Viability

Viable cell density and viability in batch cultures performed with (A) pump tubes GORE STA-PURE or PharMed, (B) ATF at different flow rates and (C) TFF at different flow rates; error bars indicate duplicate runs. Effect of flow rate and average shear rate on the cell growth in ATF and TFF systems operated at different flow rates; growth rate, average of the values at days 2 and 3, represented as function of the flow rate (D-left) and the shear rate (D-right) calculated by Equations 1 and S15 – error bars give the variation in repeated experiments listed in Material and Method. Effect of flow rate and shear rate on the average growth rate ratio (growth rate ratio = growth rate/control growth rate, where control is absence of flow 'No shear') by regression analysis (red lines) for ATF and TFF (E), and for TFF only (F) showing a strong correlation between the growth rate ratio and the flow rate or the shear rate in TFF system, as indicated by the adjusted R2 value.

Figure 2F). It showed that high shear stress decreased the growth rate, but that a low shear stress had an enhancement effect of the growth rate.

Global Cellular Response to Shear Stress

Here, we sought to characterize the global cellular response of shear stress at the transcriptome level by comparing gene expression under different conditions, i.e. filtration modes and shear rate. A list of the cultures used for the transcriptome sampling with their corresponding applied flow rate conditions is given in Table 1. Principal component analysis (PCA) showed clear differences in the overall gene expression responses to ATF, TFF, flow rate, shear stress, and cultivation time (Figures 3A and 3B). For instance, cells grown in TFF3 conditions at 0.2 L/min flow rate with two-day cultivation time (TFF3_D2) showed complete separation from those with three-day cultivation time (TFF3_D3) and ATF2_D3, all of which shared shear stress and flow rate. The TFF3_D2 samples were excluded from downstream analysis since these corresponded to a shear applied during a shorter time than three days, represented added sample heterogeneity, and showed clearly distinct responses from the remaining samples. Substantial differences were identified among all the ATF conditions in response to flow rate and shear stress, within similar cultivation time. This was the case of ATF4_D3 and ATF5_D3 at 0.5 and 0.6 L/min, which were grouped together and had similar shear stress (Table S1 - Count data and TPM data for different flow rate using ATF or TFF), and were distinct from ATF15_D3 at 0.8 L/min.

Experiment Name	Flow Rate (L/min or LPM)	Shear Rate (1/s)	Shear Stress (N/m^2)	Sample Name/ Culture day	Sample Name/ Culture day
Control	0	0	0	Control/day 2	Control
TFF3	0.19	2482	2.48	TFF3_D2/day 2	TFF3_D3/day 3
TFF6	0.38	4965	4.96	TFF6_D2/day 2	TFF6_D3/day 3
TFF12	0.7	9146	9.15	TFF12_D2/day 2	TFF12_D3/day 3
TFF13	0.5	6533	6.53	TFF13_D2/day 2	TFF13_D3/day 3
ATF2	0.2	1865	1.86	ATF2_D2/day 2	ATF2_D3/day 3
ATF1	0.3	2697	2.70	ATF1_D2/day 2	ATF1_D3/day 3
ATF4	0.5	4361	4.36	ATF4_D2/day 2	ATF4_D3/day 3
ATF5	0.6	5194	5.19	ATF5_D2/day 2	ATF5_D3/day 3
ATF6	0.7	6026	6.03	ATF6_D2/day 2	ATF6_D3/day 3
ATF15	0.8	6858	6.86	ATF15_D2/day 2	ATF15_D3/day 3

Table 1. List of the Culture Conditions and Identifiers for Samples Subjected to Transcriptomic Analysis

Further reinforcing these distinct responses, several hundreds of genes were differentially expressed between ATF, TFF and shear stress levels (FDR <0.01, Table S2 – Differential gene expression between ATF, TFF, high, low or no shear). Differentially expressed genes amount to 415 between ATF *vs.* TFF (Figures 3C), 538 between high *vs.* low shear stress, among substantial differences identified between each condition and control. These differences translated into significant alterations in biological processes (FDR <0.01; Table S3 - Significant alterations in cell biological processes between ATF, TFF, high, low or no shear), and reflected shear stress-specific responses. When compared with low shear stress, high shear stress samples display up-regulated amino acid and amide metabolism, RNA processing and transcription, unfolded protein response (UPR), ribosome biogenesis and translation, folic acid metabolism, response to ER stress such as apoptosis, response to glucose starvation. On the other hand, high shear stress samples displayed down-regulated sterol, steroid, isoprenoid and alcohol biosynthesis, cell and tissue development and morphogenesis, cell-cell adhesion and signaling and lipid biosynthetic process (FDR <0.005, Figure 3D). Additionally, high and low shear rate showed up-regulation of processes associated with cell cycle proliferation and mitosis, chromosome segregation (FDR <0.005) when compared with controls (Table S3). TFF samples with high shear stress displayed up-regulated cell cycle proliferation and response to stress (Figures 3E and Table S3) in comparison with ATF samples. This corroborated the observation of Figure 2D that the growth rate significantly decreased with the shear rate in TFF samples while this trend was less marked in ATF samples. Furthermore the metabolic processes were up-regulated for these latter. This point will be discussed below with the analysis of the glucose metabolism in "Effect of the shear rate on the cell metabolism".

Shear Stress-Related Cytoskeleton/Cell Adhesion Reorganization and Cell Death

As seen in Figure 3F, several shear stress-specific genes with TPM value > 1 could be identified. For each condition, specific on/off genes related to cytoskeleton, cell adhesion and morphogenesis were found. For instance, DCN (decorin), COL23A1, COL16A1, COL5A1, WTIP, CDH8, SBK2, NKX23, PTPRB, PSTPIP1, ESAM, CDH8, SNED1, and PCDHB11 were suppressed by high shear stress (found under normal and low shear rate), whereas SYNPO, CXCL1, ARC, PRR4, SRPX2, AOC3, CD72, ITGAX, and KLHL10 were expressed under high shear stress (Table S4 - Genes expressed at specific shear stress levels: low, high, no shear, or high and low). Furthermore, some of the genes were related to immune and inflammatory response. Besides, some of the cytoskeleton and morphogenesis genes showed expression just in the low shear stress group and included COL4A4, COL19A1, ICAM2, COL14A1, LAMB3, ITGB3, SCIN, FRY, CORO2B, MYO7A, FGD5, NUAK2, PFN4, and NTF3. Additionally, the gene set enrichment analysis showed that the expression of the genes associated with cell development and morphogenesis was down-regulated in high shear stress groups (Figure 3D).

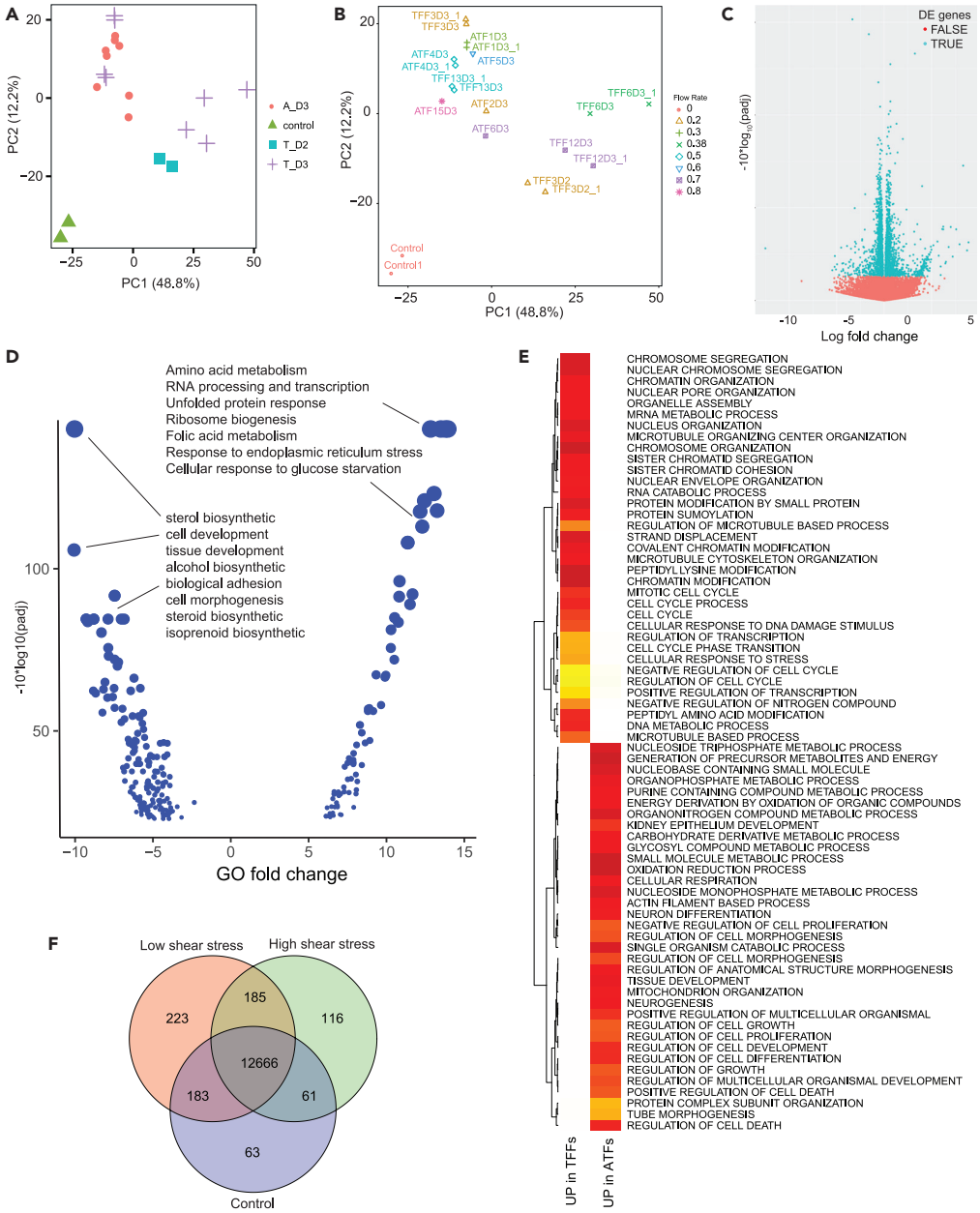

Figure 3. Cells Display Distinct Gene Expression Responses to Shear Stress

(A) PCA of Log_2-normalized gene expression in control, ATF cultivated for 3 days (ATF_D3), and TFF cultivated for 2 (TFF_D2) or 3 (TFF_D3) days.

(B) PCA with respect to different flow rates.

(C) Differentially expressed genes (cyan, FDR <0.05) and non-differentially expressed genes (red) as function of Log_2-fold change differences, between ATF and TFF.

(D) Enriched biological processes (FDR <0.005) as function of biological process change, for the comparison between high and low shear stress. Dot sizes are proportional to the significance.

(E) Biological processes exclusively up-regulated (FDR <0.001) in TFF and ATF. Colors indicate up-regulation strength, from least (yellow) to most (red) enriched terms.

(F) Venn diagram illustrating genes with TPM value > 1 for low, high, and control shear stress conditions – Data in Tables S1, S2, S3, and S4

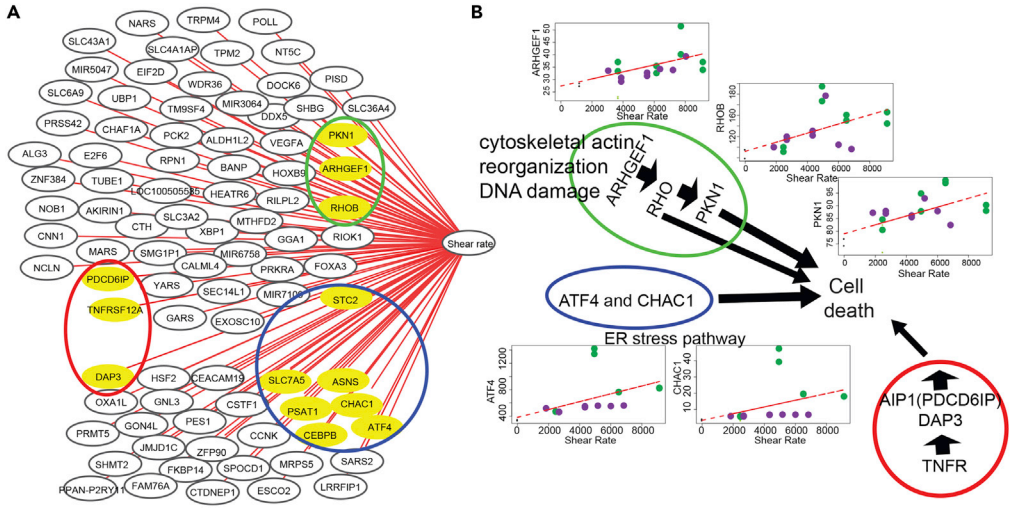

Figure 4. Association between Gene Expression and Shear Stress

(A) Genes with expression correlated with the shear stress, highlighting three groups of genes associated with apoptosis detailed in the right panel. (B) Apoptosis pathways associated with shear stress; cytoskeleton reorganization and DNA damage, ER stress pathway and extrinsic signal-induced cell death. Data in Tables S5.

We then computed pairwise Spearman rank correlations between gene expression (TPM values) and sample metadata to identify potential relationships between metadata and co-regulated or functionally associated genes (highest Spearman's ρ 0.7, FDR $<10^{-4}$). Figure 4A shows the association between gene expression and shear stress and Figure 4B illustrates the apoptosis pathways associated with shear stress. Among the significantly correlated genes, three groups were identified to be associated with apoptosis. The first group included ARHGEF1, RHOB and PKN1, which are shear stress-correlated genes and are represented in Figure 4B. These are associated with cytoskeleton reorganization and DNA damage (Table S5 – List of genes with expression associated with shear stress). They may trigger apoptosis through the activation of RhoB, a small GTPase regulating cytoskeletal reorganization and cell growth (Prendergast, 2001; Liu et al., 2001; Price and Collard, 2001; Kim et al., 2009). The second group included TNFR, DAP3, and PDCD6IP, genes associated with extrinsic signal-induced cell death (Rauert et al., 2011). The third group included genes involved in response to ER including UPR such as ATF4_gene, CHAC1, and CEBPB. UPR can be stimulated by several physiological changes including glucose shortage, hypoxia and genome instability, processes identified above through gene enrichment analysis. These genes are tightly co-regulated, for example, CEBPB controls ATF4_gene expression, which in turn regulates expression of CHAC1, a proapoptotic ER stress protein (Crawford et al., 2015) (Figure 4B). Because UPR may also be initiated in response to amino acid limitation (Su and Kilberg, 2008), we computed amino acid usage in the culture by quantifying their cell-specific consumption rate. Polynomial regression analysis showed that the consumption of all the amino acids except glutamine and alanine was weakly associated with the shear rate in ATF and had a strong correlation with the shear rate in TFF (Figure S3). Interestingly, differential expression analysis showed that the above-mentioned genes were significantly expressed in high, but not in low shear stress conditions. Overall, all observations indicated that high shear stress stimulated apoptosis associated with ER stress, cytoskeleton reorganization, and extra-cellular pathway.

Effect of the Shear Rate on the Cell Metabolism

Figures 5A–5D show the cell specific rates of glucose consumption, q_{gluc}, and lactate production, q_{lac}, as function of increasing flow rate and shear rate in TFF and ATF systems. Both q_{gluc} and q_{lac} first decreased with increasing flow rates until 0.38 L/min and 0.6 L/min for the TFF and the ATF systems, respectively. It then increased with increasing flow rate. When representing q_{gluc} and q_{lac} as function of the shear rate, the trends for both systems were comparable with a threshold $\gamma_{threshold}$ of 4900 s^{-1} (or shear stress threshold $\tau_{threshold}$). For shear rates $< \gamma_{threshold}$, q_{gluc} and q_{lac} decreased with the shear rate while this parameter had a tendency to increase again for shear rates $> \gamma_{threshold}$. Two regions separated by $\gamma_{threshold}$ (or) $\tau_{threshold}$ were thus observed: a low shear region where q_{gluc} and q_{lac} decreased with increasing shear stress, and high shear region where q_{gluc} and q_{lac} tended to increase with increasing shear stress. The ratio of q_{lac} over q_{gluc} represented in Figures 5E and 5F indicated that q_{lac}/q_{gluc} was stable for shear rates $< \gamma_{threshold}$ and

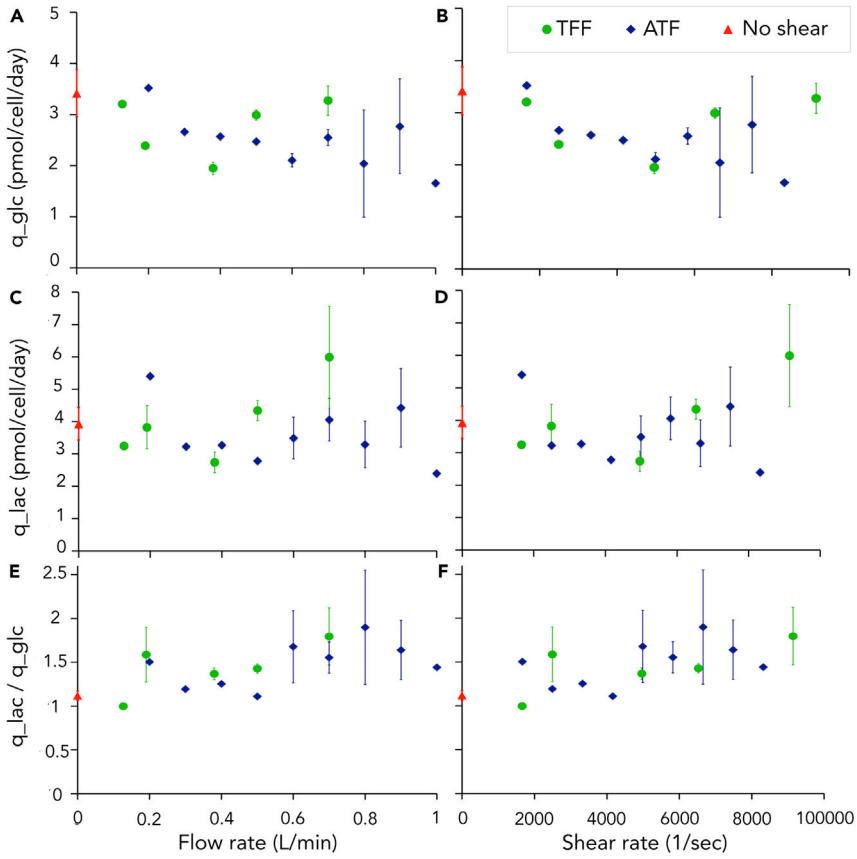

Figure 5. Effect of Different Flow Rates in ATF and TFF Systems on the Cell Specific Glucose Consumption Rate, q_{gluc}, the Cell Specific Lactate Production Rate, q_{lac}, and the Ratio q_{lac}/q_{gluc}

(A) q_{gluc} as function of the flow rate.

(B) q_{gluc} as function of the shear rate calculated by Equations 1 and S15.

(C) q_{lac} as function of the flow rate.

(D) q_{lac} as function of the shear rate.

(E) q_{lac}/q_{gluc} as function of the flow rate.

(F) q_{lac}/q_{gluc} as function of the shear rate – all rates were averages of the values at days 2 and 3; the error bars give the variation in repeated experiments and control is absence of flow 'No shear'

increasing with the flow rate and shear rate (or shear stress) for shear rates > $\gamma_{threshold}$. This tendency was significant (p value 0.0147) according to pump had an operating range *t* test for q_{lac}/q_{gluc} separated in these two regions, i.e. shear rates < $\gamma_{threshold}$ and shear rates > $\gamma_{threshold}$.

DAVID was used to perform an enrichment analysis (Huang et al., 2009) on the KEGG metabolic pathway. It showed that amino acid biosynthesis, folate metabolism, and aminoacyl-tRNA biosynthesis were enriched in high shear stress. Importantly, most genes involved in these pathways showed strong and positive correlations with the shear stress (Figure 4). This was the case for ALDH1L2, MTHFD1L, MTHFD2, and SHMT2 in folate metabolism, YARS, GARS, NARS, MARS, and SARS2 in Aminoacyl-tRNA biosynthesis and CTH, PSAT1, and ASNS in amino acid biosynthesis. Their overexpression under high shear stress was consistent with ER stress and ATF4_gene expression, whereas folate metabolism (through MTHFD1L, MTHFD2) was associated with response to oxidative stress (Celardo et al., 2017). An overview of the main effects of high and of low shear stress on the gene expression is given in Table 2.

Shear Stress in HEK293 as Mammalian/Human Cell Factory Increases Erythropoietin Expression

Finally, we sought to identify the effect of shear stress and cultivation parameters on the production of rhEPO. It was observed that the cultures with low shear stress, i.e. $\leq$ 5 N/m^2, ATF1_D3, ATF2_D3,

Effect of High Shear Stress	
Genes increased compared to no or low shear stress	Genes decreased compared to no or low shear stress
• Amino acid metabolism – CTH, PSAT1 and ASN • Unfolded protein response (UPR) – halting protein translation, degrading misfolded proteins, increasing chaperones involved in protein folding, eventually leading to apoptosis • Folic acid metabolism – ALDH1L2, SHMT2, and MTHFD1L, MTHFD2 ➢ Associated with response to oxidative stress – ATF4_gene ➢ Involved in UPR and mitochondrial dysfunction • Response to endoplasmic reticulum stress such as apoptosis • Response to glucose starvation • Cytoskeleton reorganization and DNA damage	• Cytoskeleton, cell adhesion, and morphogenesis • Sterol, steroid, isoprenoid, and lipid biosynthetic process
Shear stress-related cytoskeleton/cell adhesion/morphogenesis and immune/inflammation	
Genes expressed at high shear stress compared to no or low shear stress	Genes suppressed at high shear stress compared to no or low shear stress
• Actin-based cell shape and motility – SYNPO • Cytoskeleton associated protein and regulation of immune system – ARC • Cellular migration and adhesion – SRPX2 •Proline-rich protein family – PRR4 • Inflammation and chemo-attractant for neutrophils – CXCL1 • Increase inflammation – AOC3 • B-cell proliferation and differentiation – CD72 • Cell-cell interaction during inflammatory responses – ITGAX • Protein degradation – KLHL10	• Collagens – COL23A1, COL16A1, COL5A1 • Decorin, supportive collagen fibrils – DCN • Cadherin, cell adhesion – WTIP, CDH8, PCDHB11 • Fibronectin, cell adhesion, growth, migration – PTPRB • Cell adhesion; cell surface interaction – ESAM • Cell development and morphogenesis
Genes of cell adhesion, cytoskeleton, cell movement, cell growth expressed only in low shear stress (not in high shear stress or in control)	
• Collagens – COL4A4, COL19A1, COL14A1 • Intercellular adhesion molecule and immune response - ICAM2 • Integrin cell adhesion and cell surface-mediated signaling – ITGB3 • Laminin, attachment, migration and organization of cells, related to integrin pathway - LAMB3 • Organization of the microfilament network – SCIN • Actin binding and actin filament binding (cell movement) – CORO2B • Myosin (cell movement) – MYO7A	

Table 2. Overview of the Main Effects of High and of Low Shear Stress Observed on the Gene Expression

(Continued on next page)

Effect of High Shear Stress
• RAS-related (RAS promotes EGFR-mediated cell proliferation) and regulation of actin cytoskeleton – FGD5, PFN4
• Integrity if mitotic centrosomes and maintenance of spindle bipolarity in mitosis – FRY
• Protection against CD95-mediated apoptosis – NUAK2

Table 2. Continued

ATF5_D3, displayed the highest EPO mRNA expression, representing >6% of the entire protein-coding gene expression pool. Additionally, in comparison with absence of shear (control), the cultures with shear stress displayed higher EPO mRNA expression (Figure 6A). It was observed as well that large growth rates promoted higher EPO mRNA expression (Figure 6B). In turn, flow rate and shear stress in both TFF and ATF systems also promoted a higher mRNA EPO expression compared to absence of shear (control), but less pronounced at higher flow or shear rates. Altogether, this indicates that shear stress has positive effects on EPO expression, especially under low shear stress levels. We also investigated the effect of shear stress on the protein secretion systems using the genes related to secretion, glycosylation and exocytosis, by collecting the genes from MSigDB (Liberzon et al., 2015). The exact Fisher test showed that perturbations of the gene expression between low and high shear stress *vs.* control were significantly different and significantly different between high and low shear stress. Therefore, it seems that low shear stress has a positive effect on this cell line as a human cell factory.

DISCUSSION

The relationships between the flow rate and the shear rate (S3 and S4) are well established for fluids in pipes and in particular for tangential flow filters. Here for the first time, we calculated the theoretical shear rate and the shear stress in an ATF device and showed that ATF generates a lower shear stress than TFF by a factor 0.637, owing to the difference in velocity profile between TFF and ATF. This was experimentally confirmed in a comparative study of the effect of the ATF and TFF at different flow rates in parallel batch cultures of HEK293 cells equipped with HF to mimic the shear environment that the cells experience in ATF and TFF perfusion operations. It was observed that the growth rate was lower for flow rates ≥0.7 L/min for ATF and ≥0.38 L/min for TFF, indicating that high flow rates and thus high shear rates were unfavorable for the cells. The representation of the growth rate as function of the average shear stress, using the theoretical

A

EPO expression

sample	TPM	frequency
ATF1_D3	68116	6.82
ATF5_D3	66213	6.63
ATF2_D3	63999	6.40
TFF3_D3	62653	6.27
ATF4_D3	60439	6.05
ATF6_D3	55956	5.60
ATF15_D3	55184	5.52
TFF6_D3	52885	5.29
TFF13_D3	52740	5.28
TFF12_D3	50706	5.07
TFF3_D2	45950	4.60
Control	41738	4.18

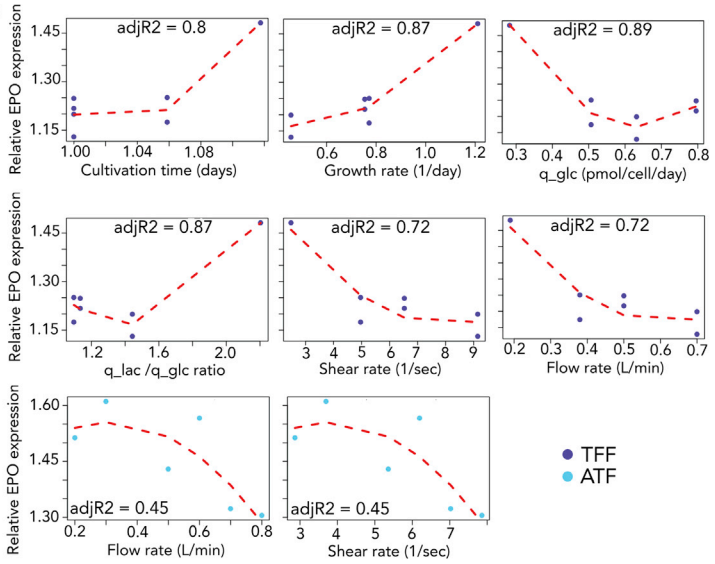

Figure 6. Effect of Cultivation Parameters on EPO Production in HEK293 Cells

(A) EPO mRNA expression (TPM) and relative expression with respect to global protein-coding gene expression

(B) Relative mRNA EPO expression (with respect to control EPO expression) and relation with culture parameters. Dark blue indicates TFF (top and middle rows), and cyan indicates ATF (bottom row)

result of Equation 1, showed a satisfying agreement of the trends obtained with ATF and with TFF. This experimentally confirmed that a lower shear stress is encountered in the HF in ATF mode compared to TFF and confirmed the theoretical relationship of the shear stress $\tau_{ATF} = 0.637\ \tau_{TFF}$ of Equation 1.

To decouple the effect of the shear in the TFF HF from the effect of the peristaltic pumping, a preliminary study was dedicated to the selection of a pump tubing that did not harm the cells. Severe cell damage was observed using the PharMed tube, whereas the cells were not affected by pumping using a GORE STA-PURE tube. It is strongly suggested that the cell damage is attributable to the roughness of the PharMed tube inner wall surface, while the GORE STA-PURE tube has a smooth inner wall surface in PTFE. Certainly, the performance of the GORE STA-PURE tubing is preferable over that of the PharMed tubing for pumping in the TFF system. The pump effect does not occur in the ATF system since a diaphragm pump operates the cell culture re-circulation instead of a peristaltic pump as in the case of TFF.

Focusing on the cell metabolism, it was observed that the influence of the shear stress on the glucose metabolism had a biphasic behavior with two zones of low and high shear stresses separated by a shear stress threshold $\tau_{threshold}$. In the low shear stress region, the cell specific glucose uptake rate, q_{gluc}, and lactate production rate, q_{lac}, decreased with the shear stress and the flow rate, while these metabolic rates increased above the shear stress threshold $\tau_{threshold}$. Interestingly, the same behavior and shear stress threshold, $\tau_{threshold}$, were observed in the case of both ATF and TFF. This also confirmed the theoretical relationship Equation 1 of the average shear stresses occurring in these devices. This biphasic behavior can be interpreted as follows. For $\tau \leq \tau_{threshold}$ the cells benefit of the shear stress, such that higher shear rate induces a more efficient glucose metabolism. However, for $\tau \geq \tau_{threshold}$ the cells are adversely impacted by increasing shear stress, demonstrated by a higher metabolic rate, i.e. higher q_{gluc} and higher q_{lac}, and increased mRNA expression of genes associated with apoptosis.

The EDR takes into account all potential types of fluid stress. This parameter is commonly used to characterize hydrodynamic conditions, in particular to evaluate the potential cell damage in bioprocesses (Chalmers, 2015). To compare the presently observed effects with the literature, the EDR in a hollow fiber for an example of 1L/min flow rate was calculated (Equation S11 Supplemental Information - Transparent Methods - Section A.2. and Figure S2), and compared to the work of Ma et al. (Ma et al., 2002) and Mollet et al. (Mollet et al., 2007) in Figure 7. For this flow rate, the EDR ranged between the dotted red lines drawn in Figure 7, in which $\tau_{threshold}$ is indicated by a red star. These values were in the same range as previously published work, reported by Mollet et al. (Mollet et al., 2004), about a 0.1 L/min flow through a 1 mm diameter pipe and the flow through in a 200 μL micropipette tip, respectively, marked items 9 and 10 in Figure 7. Although these were performed in different conditions than reported here, these numbers were in agreement with the present findings. These EDR values were significantly lower than the lethal levels reviewed by Chalmers (Chalmers, 2015) for different established cell lines. They were however potentially in the range where non-lethal effects can occur as, for instance, observed by Keane et al. (Keane et al., 2003), who showed that increasing shear stress caused a decrease in the production of recombinant human growth hormone in CHO cells accompanied by increased glucose consumption and decreased lactate production. For high shear stress, the first two effects were observed in the present study to the contrary of the lactate production, which increased here. Notice that to our knowledge, no data of the effect of mechanical shear on HEK293 cells have been reported. Under stress conditions, it can be postulated that the cells require rapid access to energy, which is corroborated by the presently observed ratio q_{lac}/q_{gluc} increasing with the shear rate for $\tau \geq \tau_{threshold}$, due to a higher glycolysis and increased lactate production, i.e. Warburg effect, instead of oxidative phosphorylation (i.e. Krebs cycle). This increased Warburg effect cannot be attributed to depletion in oxygen since the higher shear rates coincide with a shorter residence time in the cell separation device. Both for TFF and ATF, higher flow rates generate a higher number of cycles per time unit, a higher shear rate and a shorter exposure time to shear per cycle compared to lower flow rates.

Detrimental effects of high shear stress causing cell apoptosis have been previously described (Chalmers, 2015). Interestingly, we reveal here that high shear stress stimulates apoptosis associated with three pathways associated with ER stress, cytoskeleton reorganization, and extra-cellular pathway. We previously revealed oxidative stress at very high cell densities, which could be due to a higher shear stress (Zamani et al., 2018). This is consistent with the present observation of the Gene set enrichment results, where oxidative stress, folate metabolism, and UPR increased with high shear stress. Additionally, many genes involved in these pathways showed strong and positive correlations with shear stress. Folate metabolism (through MTHFD1L, MTHFD2) being associated with responses to oxidative stress is connected to ATF4_gene

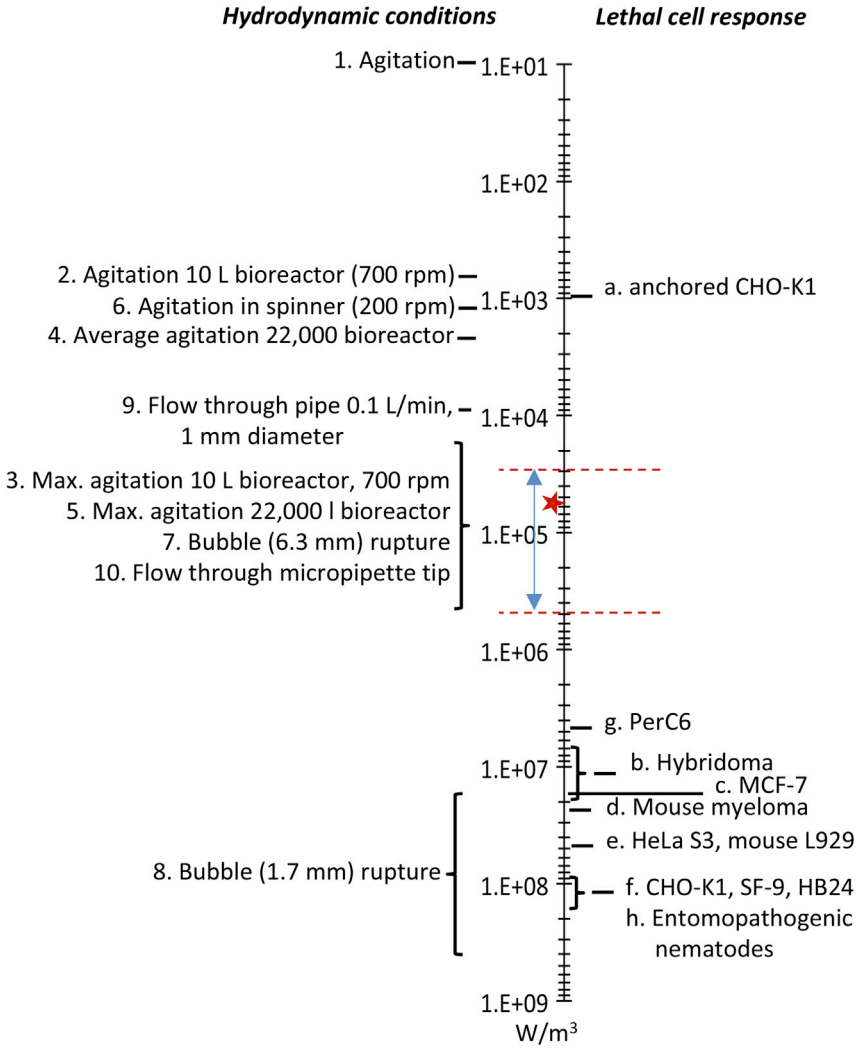

Figure 7. Energy Dissipation Rate Generated by Various Hydrodynamic Effects

Energy dissipation rate generated by various hydrodynamic effects reproduced with format adaptation from Mollet et al. (2007), where the range of the energy dissipation rate for a 1 L/min flow rate (calculated for the passage through the lumen of a hollow fiber of a cartridge CFP-4-E–3MA of 13 fibers and fiber lumen of 1 mm [General Electric Healthcare]) is given between the red dotted lines; the five-pointed star indicates the threshold shear rate $\gamma_{threshold}$ identified in this study for HEK293 cells at 4900 s^{-1}. Detailed definitions: (1) Agitation – Volume average in typical animal cell bioreactor (Varley and Birch, 1999); (2) Agitation – Volume average in a 10 L mixing vessel, RT 700 RPM (Zhou and Kresta, 1996); (3) Agitation – Maximum in a 10 L mixing vessel, RT 700 RPM (Zhou and Kresta, 1996); (4) Agitation – Volume average in a 22,000 L mixing vessel, RT 240 RPM (Wernersson and Tragarch, 1999); (5) Agitation – Maximum in the 22,000 L mixing vessel, RT 240 RPM (Wernersson and Tragarch, 1999); (6) Agitation – Maximum in spinner vessel, 200 RPM (Venkat et al., 1996); (7) Bubble rupture – Pure water bubble diameter: 6.32 mm (Garcia-Briones et al., 1994); (8) Bubble rupture – Pure water, bubble diameter: 1.7 mm (Boulton-Stone and Blake, 1993; Garcia-Briones et al., 1994); (9) Flow through pipe – Pure water, 100 mL/min, 1 mm diameter (Mollet et al., 2004); (10) Flow through a micropipette tip – Flow through a 200 μL micropipette tip in 0.2 s (Mollet et al., 2004)

expression (Celardo et al., 2017). ATF4_gene expression is also involved in the UPR (Crawford et al., 2015) and mitochondrial dysfunction (Melber and Haynes, 2018). Expression of genes associated with UPR and cell stress is elevated under high shear stress conditions, while low shear stress has a positive effect on the cells with higher expression of genes associated with cellular processes, such as transcription, cell cycle, protein phosphorylation and cell division. The aforementioned biological processes steadily increased with shear stress, so that they are substantially up-regulated under high shear stress in comparison with low shear stress where the cells showed increased response to stress (Table S3).

Importantly, we revealed that low shear stress increased the production of the recombinant protein transcription, here rhEPO. To our knowledge, this favorable effect of a mild shear stress has not been reported for stable recombinant cell lines, but it can be interesting to relate this effect with known beneficial effects of mild shear on primary or stem cells. For instance, cell proliferation and protein production increased in human tendon fibroblasts subjected to stretching (Wang and Thampatty, 2006); bovine pulmonary artery endothelial cells exhibited cell proliferation and release of bFGF when subjected to hydrostatic pressure (Wang and Thampatty, 2006); in a vascularization study, low shear stress promoted the proliferation of endothelial progenitor cells and embryonic stem cells, and enhanced their ability to form new vessels (Yamamoto and Ando, 2010); finally, shockwaves are known to reduce wound size, to increase the neo- or revascularization, increase proliferation and reduce apoptosis (Huang et al., 2013). Although an increased cell growth was not observed in the present study, the increased rhEPO transcript at low shear rate could be mediated by a comparable mechanism to primary or stem cells.

In conclusion, we have studied the shear stress effect in two TFF systems (ATF and TFF) for perfusion processes of HEK293 cells secreting EPO. Firstly, a theoretical relationship of the average shear stress in the ATF and the TFF systems, $\gamma_{ATF} \approx 0.637\gamma_{TFF}$ was established. Then, experimental investigation identified a shear stress threshold, common for ATF and TFF systems, above which reduced cell growth and altered cell metabolism were observed for HEK293 cells.

There is an increasing interest in upstream perfusion processes as part of the strategies to implement continuous manufacturing processes for economic, commercial production of therapeutic proteins (Patil and Walther, 2017). Numerous perfusion processes have already been successfully operated for CHO cells with ATF or TFF systems (Clincke et al., 2013a, 2013b), enabled by the robust nature of CHO cells. However, other more fragile cell types are emerging as important cell factories to enable the production of complex proteins that require specific post-translational modifications or are difficult-to-express in CHO cells (Tegel et al., 2020). Therefore, a better understanding of the shear stress level and its effect on cells such as HEK293 is important. Here, we have shown that a high shear stress provokes not only reduced cell growth but also a modified metabolism. However, mild shear stress can be favorable for the production of recombinant protein. Furthermore we characterized the different cell-shear interaction regions and deepened the understanding of the cells cultured in hollow fiber-based perfusion systems. We anticipate that the phenomena observed here are also likely to be occurring in other cell types and we believe these learning's should allow for improved design of new perfusion processes.

LIMITATIONS OF THE STUDY

The present study reveals a shear rate threshold, which is common for the ATF and TFF cell separation devices. It can however be observed that the detrimental effect on the cell growth of the high shear rate is more accentuated for the TFF system than for the ATF. It is unclear why this takes place since the effect of the peristaltic pump has been annihilated and, for the highest flow rate of the TFF experiments, the diaphragm pump of an ATF is used in a setting adapted for TFF. A difference, which is difficult to eliminate in this comparison, is the fact that in the ATF setting, there is only a short tube between the bioreactor and the hollow fiber cartridge, while in the TFF the connection, i.e. connection of the pump feeding the hollow fiber cartridge, is more intricate. Compared to the present small-scale system, the effect of these connections is expected to be milder in large scale due to a higher volume to wall surface ratio for the cell suspension passing the connectors and tubes.

Another aspect is that in order to generate a comparison of a large range of conditions, the present study was performed in batch mode during a time period of 5 days with cells rapidly growing in the control. A limitation is that high cell density perfusion exposes the cells to shear during a much longer time period of at least 4 weeks and most often at lower growth rate (Clincke et al., 2013b). Future investigations could address the effect of repeated shear stress and the interaction with lower growth rate in perfusion mode.

Resource Availability

Lead Contact

Veronique Chotteau (chotteau@kth.se), who should be contacted as main contact and to request further information about the protocols used, while Adil Mardinoglu (adilm@kth.se) should be contacted for bioinformatics matters.

Data and Code Availibility

The data are provided in Tables S1, S2, S3, S4, and S5; and can be found online at Mendeley Data: https://doi.org/10.1016/j.isci.2020.101653.

Materials Availability

The culture medium is commercially available. The cell line is propriety of Johan Rockberg's lab (johan.rockberg@biotech.kth.se).

METHODS

All methods can be found in the accompanying Transparent Methods supplemental file.

SUPPLEMENTAL INFORMATION

Supplemental Information can be found online at https://doi.org/10.1016/j.isci.2020.101653.

ACKNOWLEDGMENTS

This work has been carried out at the Wallenberg Center for Protein Research with co-funding of the Knut and Alice Wallenberg Foundation and AstraZeneca. Thank you as well to Dr. Jeong Lee and Dr. Luigi Grassi, both from AstraZeneca, for revising the manuscript and for their insightful inputs.

AUTHOR CONTRIBUTIONS

Conceptualization, V.C.; Methodology, C.Z., R.F., R.T., J.R., and V.C.; Investigation, C.Z., G.B., H.S., M.M., Am.M., R.F., R.T., D.H., P.V., Ad.M., J.R., and V.C.; Formal Analysis: C.Z., G.B, Ad.M. and V.C. Writing, C.Z., G.B., H.S., M.M., Am.M., R.F., R.T., D.H., P.V., Ad.M., J.R., and V.C.; Supervision, J.R., Ad.M., R.F., R.T., D.H., P.V., and V.C.

DECLARATION OF INTERESTS

G.B. is currently employee of AIVIVO Ltd, UK. C.S. and P.V. are currently employees of Kymab Ltd, UK.

Received: November 25, 2019
Revised: August 7, 2020
Accepted: October 5, 2020
Published: November 20, 2020

REFERENCES

Boulton-Stone, J.M., and Blake, J.R. (1993). Gas bubbles bursting at a free surface. J. Fluid Mech. *254*, 437–466.

Castilho, L.R., and Medronho, R.A. (2002). Cell retention devices for suspended-cell perfusion cultures. In Tools and Applications of Biochemical Engineering Science, K. Schügerl and A.P. Zeng, eds. (Springer Berlin Heidelberg), pp. 129–169.

Celardo, I., Lehmann, S., Costa, A.C., Loh, S.H., and Martins, L.M. (2017). dATF4 regulation of mitochondrial folate-mediated one-carbon metabolism is neuroprotective. Cell Death Differ. *24*, 638–648.

Chalmers, J.J. (2015). Mixing, aeration and cell damage, 30+ years later: what we learned, how it affected the cell culture industry and what we would like to know more about. Curr. Opin. Chem. Eng. *10*, 94–102.

Chalmers, J.J., and Ma, N. (2015). Hydrodynamic damage to animal cells. In Animal Cell Culture, M. Al-Rubeai, ed. (Springer, Cham.), pp. 169–183.

Chotteau, V. (2015). Perfusion processes. animal cell culture. In Animal Cell Culture, M. Al-Rubeai, ed. (Springer, Cham), pp. 407–443.

Clincke, M.F., Mölleryd, C., Samani, P.K., Lindskog, E., Fäldt, E., Walsh, K., and Chotteau, V. (2013a). Very high density of Chinese hamster ovary cells in perfusion by alternating tangential flow or tangential flow filtration in WAVE bioreactor™—part II: applications for antibody production and cryopreservation. Biotechnol. Prog. *29*, 768–777.

Clincke, M.F., Mölleryd, C., Zhang, Y., Lindskog, E., Walsh, K., and Chotteau, V. (2013b). Very high density of CHO cells in perfusion by ATF or TFF in WAVE bioreactor™. Part I. Effect of the cell density on the process. Biotechnol. Prog. *29*, 754–767.

Crawford, R.R., Prescott, E.T., Sylvester, C.F., Higdon, A.N., Shan, J., Kilberg, M.S., and Mungrue, I.N. (2015). Human CHAC1 protein degrades glutathione, and mRNA induction is regulated by the transcription factors ATF4 and ATF3 and a bipartite ATF/CRE regulatory element. J. Biol. Chem. *290*, 15878–15891.

Gálvez, J., Lecina, M., Solà, C., Cairó, J.J., and Gòdia, F. (2012). Optimization of HEK-293S cell cultures for the production of adenoviral vectors in bioreactors using on-line OUR measurements. J. Biotechnol. *157*, 214–222.

Garcia-Briones, M.A., and Chalmers, J.J. (1994). Flow parameters associated with hydrodynamic cell injury. Biotechnol. Bioeng. *44*, 1089–1098.

Garcia-Briones, M.A., Brodkey, R.S., and Chalmers, J.J. (1994). Computer Simulations of the rupture of a gas bubble at a gas-liquid interface and its implications in animal cell damage. Chem. Eng. Sci. *49*, 2301–2320.

Gomez, N., Barkhordarian, H., Lull, J., Huh, J., GhattyVenkataKrishna, P., and Zhang, X. (2019). Perfusion CHO cell culture applied to lower aggregation and increase volumetric productivity for a bispecific recombinant protein. J. Biotechnol. *304*, 70–77.

Gregoriades, N., Clay, J., Ma, N., Koelling, K., and Chalmers, J.J. (2000). Cell damage of microcarrier cultures as a function of local energy dissipation

created by a rapid extensional flow. Biotechnol. Bioeng. *69*, 171–182.

Huang, D.W., Sherman, B.T., and Lempicki, R.A. (2009). Bioinformatics enrichment tools: paths toward the comprehensive functional analysis of large gene lists. Nucleic Acids Res. *37*, 1–13.

Huang, C., Holfeld, J., Schaden, W., Orgill, D., and Ogawa, R. (2013). Mechanotherapy: revisiting physical therapy and recruiting mechanobiology for a new era in medicine. Trends Mol. Med. *19*, 555–564.

Keane, J.T., Ryan, D., and Gray, P.P. (2003). Effect of shear stress on expression of a recombinant protein by Chinese hamster ovary cells. Biotechnol. Bioeng. *81*, 211–220.

Kim, D.M., Chung, K.S., Choi, S.J., Jung, Y.J., Park, S.K., Han, G.H., Ha, J.S., Song, K.B., Choi, N.S., Kim, H.M., et al. (2009). RhoB induces apoptosis via direct interaction with TNFAIP1 in HeLa cells. Int. J. Cancer *125*, 2520–2527.

Kumar, S.R. (2015). Industrial production of clotting factors: challenges of expression and choice of host cells. Biotechnol. J. *10*, 995–1004.

Lalonde, M.E., and Durocher, Y. (2017). Therapeutic glycoprotein production in mammalian cells. J. Biotechnol. *251*, 128–140.

Liberzon, A., Birger, C., Thorvaldsdóttir, H., Ghandi, M., Mesirov, J.P., and Tamayo, P. (2015). The Molecular Signatures Database (MSigDB) hallmark gene set collection. Cell Syst. *1*, 417–425.

Liu, A.X., Rane, N., Liu, J.P., and Prendergast, G.C. (2001). RhoB is dispensable for mouse development, but it modifies susceptibility to tumor formation as well as cell adhesion and growth factor signaling in transformed cells. Mol. Cell Biol. *21*, 6906–6912.

Llop, E., Gutiérrez-Gallego, R., Segura, J., Mallorquí, J., and Pascual, J.A. (2008). Structural analysis of the glycosylation of gene-activated erythropoietin (epoetin delta, Dynepo). Anal. Biochem. *383*, 243–254.

Ma, N., Koelling, K.W., and Chalmers, J.J. (2002). Fabrication and use of a transient contractional flow device to quantify the sensitivity of mammalian and insect cells to hydrodynamic forces. Biotechnol. Bioeng. *80*, 428–437.

Melber, A., and Haynes, C.M. (2018). UPR(mt) regulation and output: a stress response mediated by mitochondrial-nuclear communication. Cell Res. *28*, 281–295.

Merten, O.W., Manuguerra, J.C., Hannoun, C., and Van der Werf, S. (1999). Production of influenza virus in serum-free mammalian cell cultures. Dev. Biol. Stand. *98*, 23–37.

Mollet, M., Godoy-Silva, R., Berdugo, C., and Chalmers, J.J. (2007). Acute hydrodynamic forces and apoptosis: a complex question. Biotechnol. Bioeng. *98*, 772–788.

Mollet, M., Ma, N., Zhao, Y., Brodkey, R., Taticek, R., and Chalmers, J.J. (2004). Bioprocess equipment: characterization of energy dissipation rate and its potential to damage cells. Biotechnol. Prog. *20*, 1437–1448.

Patil, R., and Walther, J. (2017). Continuous manufacturing of recombinant therapeutic proteins: upstream and downstream technologies. In New Bioprocessing Strategies: Development and Manufacturing of Recombinant Antibodies and Proteins, B. Kiss, U. Gottschalk, and M. Pohlscheidt, eds. (Springer, Cham), pp. 277–322.

Prendergast, G.C. (2001). Actin' up: RhoB in cancer and apoptosis. Nat. Rev. Cancer *1*, 162–168.

Price, L.S., and Collard, J.G. (2001). Regulation of the cytoskeleton by Rho-family GTPases: implications for tumour cell invasion. Semin. Cancer Biol. *11*, 167–173.

Rauert, H., Stühmer, T., Bargou, R., Wajant, H., and Siegmund, D. (2011). TNFR1 and TNFR2 regulate the extrinsic apoptotic pathway in myeloma cells by multiple mechanisms. Cell Death Dis. *2*, e194.

Shevitz, J. (2000). Fluid filtration system. US Patent *6*, 424.

Su, N., and Kilberg, M.S. (2008). C/EBP homology protein (CHOP) interacts with activating transcription factor 4 (ATF4) and negatively regulates the stress-dependent induction of the asparagine synthetase gene. J. Biol. Chem. *283*, 35106–35117.

Swiech, K., Picanço-Castro, V., and Covas, D.T. (2012). Human cells: new platform for recombinant therapeutic protein production. Protein Expr. Purif. *84*, 147–153.

Takamatsu, H., Hamamoto, K., Ishimura, K., Yokoyama, S., and Tokashiki, M. (1996). Large-scale perfusion culture process for suspended mammalian cells that uses a centrifuge with multiple settling zones. Appl. Microbiol. Biotechnol. *45*, 454–457.

Tegel, H., Dannemeyer, M., Kanje, S., Sivertsson, Å., Berling, A., Svensson, A.S., Hober, A., Enstedt, H., Volk, A.L., Lundqvist, M., et al. (2020). High throughput generation of a resource of the human secretome in mammalian cells. New Biotechnol. *58*, 45–54.

Varley, J., and Birch, J. (1999). Reactor design for large scale suspension animal cell culture. Cytotechnology *29*, 177–205.

Venkat, R.V., Stock, L.R., and Chalmers, J.J. (1996). Study of hydrodynamics in microcarrier culture spinner vessels: a particle tracking velocimetry approach. Biotechnol. Bioeng. *49*, 456–466.

Voisard, D., Meuwly, F., Ruffieux, P.A., Baer, G., and Kadouri, A. (2003). Potential of cell retention techniques for large-scale high-density perfusion culture of suspended mammalian cells. Biotechnol. Bioeng. *82*, 751–765.

Wang, J.H.C., and Thampatty, B.P. (2006). An introductory review of cell mechanobiology. Biomech. Model. Mechanobiol. *5*, 1–16.

Wang, M.D., Yang, M., Huzel, N., and Butler, M. (2002). Erythropoietin production from CHO cells grown by continuous culture in a fluidized-bed bioreactor. Biotechnol. Bioeng. *77*, 194–203.

Wernersson, E.S., and Tragarch, C. (1999). Scaleup of Rushton turbine agitated tanks. Chem. Eng. Sci. *54*, 4245–4256.

Woodside, S.M., Bowen, B.D., and Piret, J.M. (1998). Mammalian cell retention devices for stirred perfusion bioreactors. Cytotechnology *28*, 163–175.

Yamamoto, K., and Ando, J.J. (2010). Differentiation of stem/progenitor cells into vascular cells in response to fluid mechanical forces. J. Biorheol. *24*, 1.

Zamani, L., Lundqvist, M., Zhang, Y., Aberg, M., Edfors, F., Bidkhori, G., Lindahl, A., Mie, A., Mardinoglu, A., Field, R., et al. (2018). High cell density perfusion culture has a maintained exoproteome and metabolome. Biotechnol. J. *13*, 1800036.

Zhou, G., and Kresta, S.M. (1996). Distribution of energy dissipation between convective and turbulent flow for three frequently used impellers. Trans. Inst. Chem. Eng. *74*, 379–389.

Zhu, J. (2012). Mammalian cell protein expression for biopharmaceutical production. Biotechnol. Adv. *30*, 1158–1170.

iScience, Volume *23*

Supplemental Information

Low Shear Stress Increases Recombinant Protein Production and High Shear Stress Increases Apoptosis in Human Cells

Caijuan Zhan, Gholamreza Bidkhori, Hubert Schwarz, Magdalena Malm, Aman Mebrahtu, Ray Field, Christopher Sellick, Diane Hatton, Paul Varley, Adil Mardinoglu, Johan Rockberg, and Veronique Chotteau

Figure S.1 - Evolution of the Reynolds number, the shear rate (A) and the shear stress (B) as function of different flow rates in the hollow fiber of a tangential flow filtration cartridge - Related to Section Theoretical considerations - Shear stress characterization, to Figure 1 and to Transparent Methods – A.1 Shear stress characterization: Velocity profile during one cycle in ATF (C). Shear rate (D) and shear stress (E) for ATF and TFF modes of operation as function of the flow rate

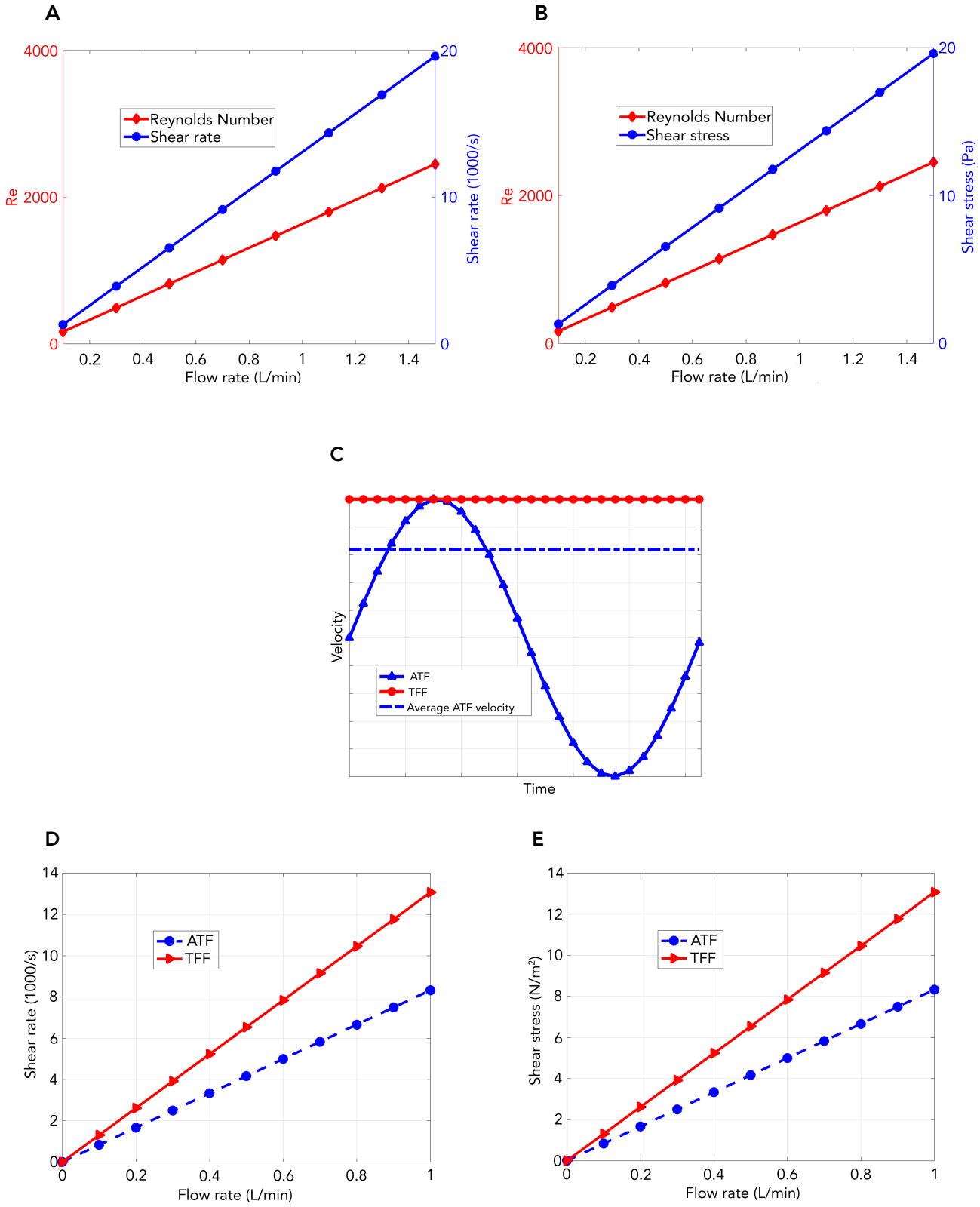

Figure S.2 - EDR (energy dissipation rate) generated from the passage in the hollow fiber lumen of a hollow fiber cartridge CFP-4-E-3MA of 13 fibers and fiber lumen of 1 mm (GE Healthcare), used in the present study - Related to Section Discussion, to Figure 7 and to Transparent Methods – A.2 Energy dissipation rate: (A) along the radius of the hollow fibers for three different flow rates, starting from the lumen center; (B) maximal EDR as function of the flow rate

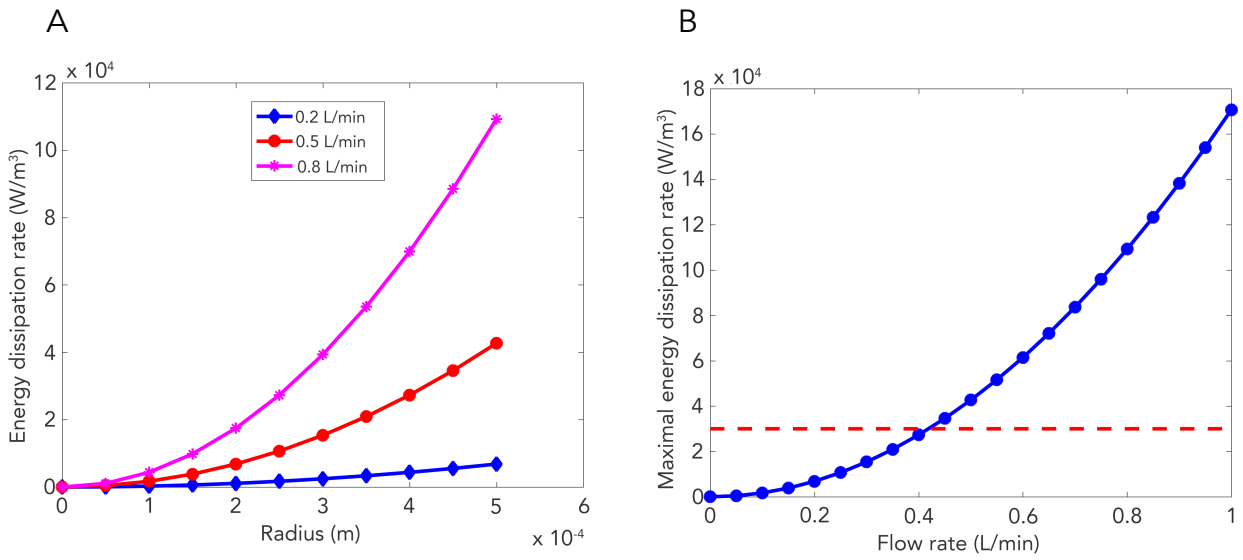

Figure S.3 – Relation between the relative cell specific amino acid consumption rate and the shear rate in TFF and ATF; relative amino acid consumption with respect to amino acid consumption in control 'No shear' (in absence of shear stress) - Related to Section Shear stress-related cytoskeleton/cell adhesion reorganization and cell death and Figure 4

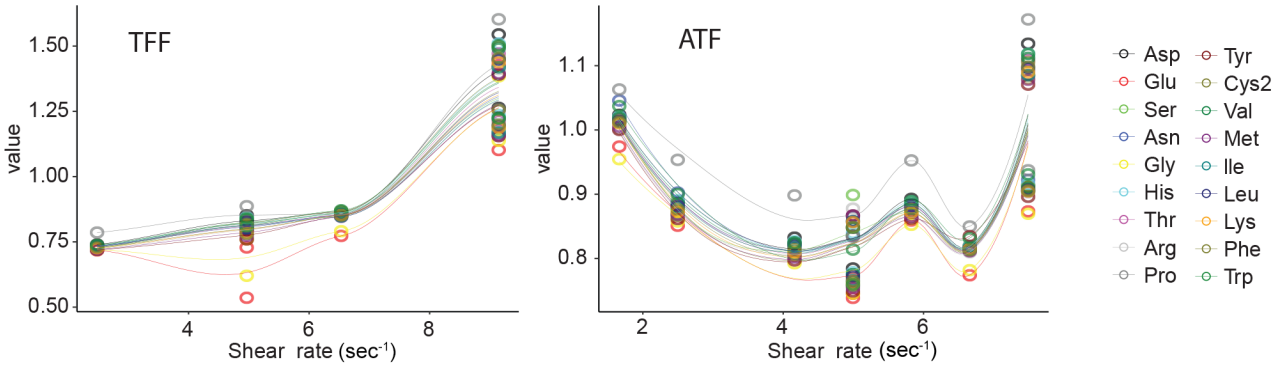

KEY RESOURCES TABLE

REAGENT or RESOURCE	SOURCE	IDENTIFIER
Antibodies		
CaptureSelect Biotin Anti-EPO Conjugate	Thermo Fisher Scientific	7103372500
Chemicals, Peptides, and Recombinant Proteins		
CD-optiCHO medium	Thermo Fisher Scientific	Cat No. 12681011
Puromycin dihydrochloride	Thermo Fisher Scientific	Cat No. A1113803
RNAlater stabilization solution	Thermo Fisher Scientific	Cat No. AM7021
Experimental Models: Cell Lines		
Human: Freestyle 293-F	Thermo Fisher Scientific	R79007
Freestyle 293-F: HEK293: EPO-HPC4-GFP11	This paper	N/A
Recombinant DNA		
pD2529-CMV	Atum	pD2529-CMV
Software and Algorithms		
PathWave	Schramm 2010	https://github.com/KoenigLabNM/Pathwave
Cytoscape	Shannon 2003	https://cytoscape.org/
PIANO	Väremo 2013	https://bioconductor.org/packages/release/bioc/html/piano.html
MSigDB	Liberzon 2015	https://www.gsea-msigdb.org/gsea/msigdb
DESeq2	Love 2014	https://bioconductor.org/packages/release/bioc/html/DESeq2.html
Kallisto	Bray 2016	https://pachterlab.github.io/kallisto/about
org.Hs.eg.db	Carlson 2019	https://bioconductor.org/packages/release/data/annotation/html/org.Hs.eg.db.html
Other		
Microfiltration hollow fiber cartridge	GE Healthcare - Cytiva	CFP-4-E-3MA

TRANSPARENT METHODS

A THEORETICAL CONSIDERATIONS

A.1 Shear stress characterization

The flow in a hollow fiber cartridge at steady state has a Poiseuille profile, i.e. the cross-section velocity has a parabolic profile. The Reynolds number, Re, can be used to predict if a flow is laminar or turbulent inside a hollow fiber.

$$Re = u\frac{L}{\nu} \tag{S.1}$$

where u is the velocity of the fluid (m/s), L is the hydraulic diameter (m) and ν is the kinematic viscosity of the fluid (m^2/s). The shear rate and shear stress in the hollow fiber can be calculated as follows

$$\gamma = \frac{\partial u}{\partial y} \tag{S.2}$$

$$\tau = \sigma\ \frac{\partial u}{\partial y} = \sigma\ \gamma \tag{S.3}$$

where γ is the shear rate, τ is the shear stress, σ is the dynamic viscosity of the fluid and $\nu = {}^{\sigma}/_{\rho}$, where ρ is the fluid density. In a pipe the shear rate is given by

$$\gamma = \frac{4\ Q_{fiber}}{\Pi\ R^3} \tag{S.4}$$

where Q_{fiber} is the flow rate in a fiber and R is the fiber radius (Selection Handbook, Cross Flow Filtration Method Handbook).

Using **Eq**. S.8 and S.9, the shear rate and shear stress were calculated for the present hollow fiber cartridge (see Material and Method) and given in Figure S.1D-E. The Reynolds number was below 2000 for flow rates below 1.0 L/min. For pipe flow, laminar flow occurs when *Re* < 1000 while turbulent flow occurs when *Re* > 2000 (Faisst and Eckhardt, 2004). In the *Re* range between 1000 and 2000, laminar and turbulent flows are possible and are called "transition" flows.

In the TFF system, the fluid velocity is constant while it varies in the ATF system with a sinusoidal profile as schematically represented in Figure S1C. This sinusoidal profile has an absolute maximum value equal to the constant fluid velocity in the TFF. This implies that the instantaneous shear rate in the ATF system is sinusoidal as well, while it is constant in the TFF system. The shear rate in the ATF system can be written as

$$\gamma = \frac{\partial u}{\partial y} = \frac{\partial U_0 \sin(\omega t)}{\partial y} = \frac{\partial U_0}{\partial y} \cdot \sin(\omega t) \tag{S.5}$$

where ω is the frequency of the ATF cycle (s^{-1}), calculated from the flow rate of the ATF. The relationship between the ATF setting flow rate and the frequency can be expressed as

$$Q = 60 \cdot V \cdot \omega \tag{S.6}$$

where Q is the flow rate (L/min) in the hollow fiber cartridge filter and V (L) is the displacement volume of the ATF diaphragm pump, i.e. the chamber volume of the ATF.

In the range 0 to π, the average shear rate in the ATF can then be expressed as a function of its maximum absolute value constantly obtained in the TFF system, as follows

$$\gamma_{ATF} = \frac{\partial \mathrm{U}_0}{\partial \mathrm{y}} \cdot \frac{\int_0^{\pi} \sin(\omega t) \cdot d\omega t}{\pi} = \gamma_{TFF} \cdot \frac{2}{\pi} \approx 0.637\gamma_{TFF} \tag{S.7}$$

where $\frac{\partial U_0}{\partial y} = \gamma_{TFF}$ is the constant shear rate occurring in the TFF.
This result implies that the average absolute shear rate is lower in the ATF than in the TFF and is $\frac{2}{\pi} \approx 0.637$ of the average shear rate in the TFF, although the instantaneous shear rate in the ATF system has a maximum equal to the constant shear rate in the TFF system.
Taking into account **Eq**. S.3 and S.7, the average shear stress in the ATF, τ_{ATF}, can be written

$$\tau_{ATF} = \tau_{TFF} \cdot \frac{2}{\pi} \approx 0.637\, \tau_{TFF} \tag{S.8}$$

where τ_{TFF} is the average shear stress in the TFF.

Figure S.1D-E gives the shear rate and the shear stress as function of the flow rate in the ATF and TFF systems. For instance, for a flow rate of 1 L/min, the shear stress in the ATF and the TFF are 8.3 and 13 N/m^2, respectively, according to **Eq**. S.4.

A.2 Energy dissipation rate

The velocity profile equation for fully developed laminar flow in a pipe (Bird 2002, Brodkey 1995) is

$$\frac{dU_z}{dr} = \frac{-4Qr}{\pi R^4} \tag{S.9}$$

where Q is the volumetric flow rate, r is the radial position, and R is the radius of the pipe.
When the fluid is a Newtonian fluid and this equation can be derived to express the EDR, ϵ as

$$\epsilon = \sigma \left(\frac{dU_z}{dr}\right)^2 = \sigma \cdot \frac{16Q^2r^2}{\pi^2 R^8} \tag{S.10}$$

The value of $\frac{dU_z}{dr}$ is largest at the wall of the pipe, where $r = R$, so the maximum local EDR in this case is

$$\epsilon_{max} = \sigma \cdot \frac{16Q^2}{\pi^2 R^6} \tag{S.11}$$

Figure S.2A-B represents the EDR as function of the radius for different flow rates and the maximal EDR as function of the flow rate, given by **Eq**. S.11.

B METHODS

B.1 Generation of EPO-producing HEK293 cell line

A monoclonal HEK293F cell line expressing human recombinant erythropoietin (rhEPO) was created as follows. The gene encoding human EPO fused to a C-terminal HPC4-tag was cloned into the pD2529 expression vector (Atum) according to manufacturer's instructions (Electra cloning system). The plasmid was linearized by PvuI restriction enzyme. Freestyle 293-F cells (Gibco, Thermo Fisher Scientific) were cultured in Freestyle 293 expression medium (Gibco, Thermo Fisher Scientific) in 125 ml Erlenmeyer shake flask with vented caps at 37°C, 125 rpm and 8% CO_2. Cells were transfected at a cell density of 0.65 x 10^6 cells/ml with 1 µg of linearized plasmid per 1 million cells using PEI as transfection reagent at a DNA:PEI w/w ratio of 1:3 with. DNA and PEI were mixed by vortexing and precomplexed at 15 min before addition to cells. Isolation of stable plasmid-integrated clones was carried out by puromycin selection at a concentration of 2 µg/ml at day 2–13 post transfection. Single EPO-producing clones were isolated by sorting of single cells into each well of a 384-well plate using FACS (Astrios, Beckman Coulter) followed by verification of single cells by microscopy (Leica DMI6000B). Cells were expanded in Freestyle 293 medium supplemented with 1.5% HEPES at 37°C and 8% CO_2. A high-producing clone was identified by biolayer interferometry as described by Kol *et al* (Kol 2015) using CaptureSelect Biotin Anti-EPO Conjugate (Thermo Fisher Scientific) and the Octet RED96 instrument (Pall ForteBio, CA, USA).

B.2 Cell culture

The cells were routinely passaged every 3 or 4 day in CD-optiCHO medium (Thermo Fisher Scientific) in shake flasks (Corning) in a 5% CO_2 incubator. The medium was supplemented with 4 mM glutamine (Fujifilm Irvine Scientific), 100 mg/L streptomycin, 60 mg/L penicillin G (both Sigma-Aldrich) and puromycin (2 µg/mL) (Thermo Fisher Scientific).

B.3 Experimental setup

Bioreactor

The experiments were performed in four identical bioreactors of a DASbox Mini Bioreactor system (Eppendorf) equipped with marine impellers. The working volume in the bioreactor was 180 mL. The hold volume for the TFF system was 20 mL while it varied between 10 and 100 mL for the ATF system. The marine impellers had 3 cm diameter and were stirred at 250 rpm. The temperature was maintained at 37°C using a heating band. The pH was maintained at 7.0 using automatic additions of carbon dioxide or 0.5 M Na_2CO_3. The dissolved oxygen concentration (DO) was controlled at 40% air saturation using air, nitrogen and oxygen automatic additions. The cell density, viability, DO, pH, osmolality, and key nutrients and metabolites were daily monitored with a NovaBioprofile Flex (Nova Biomedical, USA).
The bioreactors were inoculated with cells at passage number between 6 and 24 at density 0.5 x 10^6 cells/mL, and the cell growth was monitored during 5 days. The reference condition was the absence of re-circulation in TFF or ATF, labeled 'No shear' in the graphs. This reference condition was carried out in triplicate, with cells at passages 6, passage 22 and passage 24.

Effect of shear stress

The effect of shear stress was studied by applying tangential flow filtration or alternating tangential flow filtration as used in perfusion culture, however the culture was carried out in batch mode for 5 days. For this, the TFF and ATF were connected in the same way as these are connected for perfusion operation but no fluid was removed from the permeate side of the hollow fiber. The HF cartridge of the ATF was connected to the bioreactor with a dip tube. The same connection was

used for the TFF system where the cell broth was recycled to the bioreactor using another dip tube connection in the bioreactor head plate. In both the ATF and TFF systems, the tangential flow filtration was performed using hollow fiber cartridges (GE Healthcare - Cytiva, CFP-4-E-3MA with 13 fibers, membrane area 110 cm^2, pore size 0.45 μm, fiber lumen 1 mm, nominal low path length 30 cm). The schematic setups for TFF and ATF are shown in **Figure 1**.

ATF system

In the ATF system, the diaphragm pump of an ATF-2 device (Repligen, Refine Technology) generated an alternating flow recirculation in the HF. The operating conditions for ATF were $0.2_{(n=1)}$, $0.3_{(n=1)}$, $0.4_{(n=1)}$, $0.5_{(n=1)}$, $0.6_{(n=2)}$, $0.7_{(n=3)}$, $0.8_{(n=2)}$, $0.9_{(n=3)}$ and $1_{(n=1)}$ L/min (shear stress 1.6-7.5 N/m^2), with absence of recirculation 'No shear' as control condition, i.e. $0_{(n=3)}$ L/min, where subscript n denotes the number of repetitions per condition.

TFF system

In the TFF system, the flow was driven in one direction by a peristaltic pump Alitea XV (Watson-Marlow) for flow rate ≤ 0.38 mL/min. For this system, the pump tube was a GORE STA-PURE PCS pump tube 3/16'' ID x 5/16'' OD made of silicone in a PTFE lattice (ePTFE and platinum-cured silicone composite – Gore) or a PharMed BPT pump tube 3/16'' ID x 5/16'' OD (Saint-Gobain) in preliminary studies as detailed in the text. This pump had an operating range up to 0.19 L/min, hence to obtain a flow of 0.38 mL/min, two pumps were used in parallel and above that flow the diaphragm pump of the ATF2 system was used in combination with one-way check valves to create a flow in one direction. The operating conditions for TFF were $0.127_{(n=1)}$, $0.191_{(n=2)}$, $0.38_{(n=2)}$, $0.5_{(n=2)}$ and $0.7_{(n=2)}$ L/min (shear stress 1.6-9.1 N/m^2), with the same control conditions as ATF, i.e. $0_{(n=3)}$ L/min absence of recirculation 'No shear'.

B.4 Metabolism and product analyses

The cell growth and main metabolite concentrations were daily measured to monitor the metabolic production and consumption rates. The viable cell density, viability and concentrations of the main metabolites, glucose, lactate, glutamine and ammonia, were analyzed by Bioprofile Flex (Nova Biomedical, USA). Amino acid analysis was performed based on a Waters UPLC Amino Acid Analysis applications kit using the vendor's protocol; briefly: Cell culture supernatants were filtered through 10 kDa filters and filtrates were diluted using HPLC grade water to appropriate concentrations. Amino Acid Standard (Waters) was diluted for use as a standard curve. Diluted samples and standards were combined with internal standard Norvaline (Sigma-Aldrich) and AccQ Tag Derivatization Kit reagents (Waters). Samples were run on an Acquity UPLC system (Waters) using an AccQ-Tag Ultra RP Column 130 Å 1.7 µm, 2.1 mm, 100 mm (Waters). Data were analysed using EMPOWER software (Waters). Recombinant human erythropoietin (rhEPO) expressed by HEK293 was quantified using a sandwich ELISA kit (Invitrogen) with human erythropoietin Standard used as standard.

The cell growth rate μ_i at time $T_{i\ (i=1,\dots,5)}$ was calculated as follows

$$\mu_i = \frac{\ln\left(C_{tot_i}/C_{tot_{i-1}}\right)}{T_i - T_{i-1}} \tag{S12}$$

where C_{tot_i} is the total cell density (x 10^6 cells/mL) at time T_i.
The cell specific consumption rate of a substrate *c*, q_{c_i}, (e.g. glucose) at time T_i was calculated as

$$q_{c_i} = \frac{2\left(C_{i-1} - C_i\right)}{\left(T_i - T_{i-1}\right)\left(C_{v_i} + C_{v_{i-1}}\right)} \tag{S13}$$

where C_i is the concentration of the metabolite *c*, and C_{v_i} the cell density at time T_i.
The cell specific production rates of a product *p* (e.g. lactate, rhEPO) at time T_i, q_{p_i}, was calculated as:

$$q_{p_i} = \frac{2\ (P_i\ - P_{i-1})}{(T_i - T_{i-1})\ (C_{v_i} + C_{v_{i-1}})} \quad \text{(S14)}$$

where P_i *is* the concentration of product *p*.

For the calculation of the growth rate, as well as the cell specific consumption of glucose and production of lactate, weighted moving averaging was applied on the data. The average $\bar{x}_i$ calculated as:

$$\bar{x}_i = \frac{x_{i-1} + 2\,x_i + x_{i+1}}{4} \quad \text{(S15)}$$

was considered for **Eq S12, S13** and **S14**, where $x_{i\ (i=1,\dots,5)}$ was the cell density, the glucose concentration or the lactate concentration at sampling events T_i . The average of the specific rates at day 2 and at day 3, where exponential growth occurred, was considered.

Statistical comparisons of the metabolic rates were made using Student's t-test for unpaired samples and unequal sample sizes according to Cardillo 2006. p-values < 0.05 were considered significant and are given in the text.

B.5 RNA sample preparation and transcript profiling of HEK293 cells

For RNA extraction, 1 mL cell broth samples were collected from the bioreactors on a daily basis, centrifuged at 4°C and the cell pellet was resuspend in 200 µL RNAlater Stabilization Solution (Invitrogen, Thermo Fisher Scientific) to stabilize and preserve the cells. These were then kept at 4°C overnight and then stored at -80°C until analysis. Frozen pellets were thawed and subsequently treated as starting material for Total RNA extraction and analysis. Briefly, cells were lysed and homogenized, followed by genomic DNA removal on gDNA Eliminator spin columns and RNA Isolation on RNeasy® Spin Columns utilizing the Qiagen RNeasy® Plus Universal Mini Kit according to manufacturer's instructions (Qiagen, Germany). Quality control on extracted Total RNA prior to sequencing was performed on an Agilent Bioanalyzer 2100 system together with the Agilent RNA 6000 Nano kit (Agilent Technologies, CA, US). All samples submitted for sequencing had a RNA Integrity number (RIN) >8. They were sequenced using Illumina HiSeq 2500 High Output Mode, at paired-end 2x125bp (Illumina HiSeq platform via a commercial service of Eurofins MWG GmbH, Germany). Subsequently, we processed FASTQ files as paired-end raw sequencing data and quantify TPM and count values for transcripts by Kallisto method (Bray 2016) using cDNA human reference (GRCh38) from Ensembl release 92. We added the transcript sequence of recombinant EPO to the reference FASTA file to investigate the expression of recombinant EPO in different flow/shear rate. The gene count and TPM values were calculated from transcript level abundance and counts using R package tximport (Soneson 2015) based on Ensembl gene version 92.

B.6 Clustering Similarity Matrices, correlation, differential expression and statistical analyses

The similarity matrix for the samples were generated based on Spearman correlation regarding the log transformed TPMs. We used Hierarchical clustering with Ward.D2 and Euclidean distance to cluster the samples based on the similarity matrix.
Differential expression analyses were performed based on raw counts through R using the DESeq2 package and Wald test p value (Love 2014). Differential expression analysis was performed by

partitioning subjects according to either different bioreactor system or high *vs.* low shear rate. Genes displaying median TPM value <1 across samples were ignored.
Hypothesis testing was performed by considering the null hypothesis of absence of association between the compared variables. The statistical test for association was selected according to the nature of the data: continuous data *vs.* continuous data by Spearman rank correlation test and categorical data *vs.* categorical data by Fisher's exact test for 2x2 tables. Statistical methods are indicated and considered significant after multiple hypothesis testing (Benjamin-Hochberg) where Q < 0.05. Spearman rank correlations were computed for gene expression *vs.* cultivation parameters across samples, and Q values were used to find significant correlations as indicated throughout. Cytoscape (Shannon 2003) was used to visualize the co-expression network.

B.7 Gene set enrichment and KEGG pathway analysis

Gene set enrichment analysis (GSEA) was performed through PIANO using whole-genome Log_2 fold changes and adjusted P values attained from DESeq2 as gene-level statistics, with geneSetStat = reporter, and nPerm = 1000. Gene Ontology biological processes were downloaded from MSigDB (Liberzon 2014). Gene Ontology processes were considered as enriched with an FDR of 5%, and with clear direction (i.e. non-mixed). Additionally, we ignored Gene Ontology processes related with tissues/organs of different embryonic origin (e.g. brain, bone, hair).
Gene expression enrichment was also performed on KEGG metabolic pathways through PathWave (Schramm 2010), with 1000 permutations. Local pathways were selected if at least three reactions (or genes) were enriched in a pathway (Q < 0.05). The inputs of PathWave were TPM values for the genes having Entrez ID and the median TPM>1. For ID mapping the "org.Hs.eg.db" R package was used (Carlson 2019).

B.8 Data availability

The data are available at doi:10.17632/bb5vw384h3.1 (Mendeley data).

SUPPLEMENTAL REFERENCES

Bird, R.B. (2002), *Transport phenomena*. Applied Mechanics Reviews 55, R1-R4.

Bray, N.L., Pimentel, H., Melsted, P., Pachter, L., 2016. Near-optimal probabilistic RNA-seq quantification. Nat Biotechnol. 34(5):525-7. doi: 10.1038/nbt.3519. Epub 2016 Apr 4.

Brodkey, R.S. (1995) *The phenomena of fluid motions*. Courier Corporation.

Cardillo, G. (2006). Student t-Test for unpaired or paired samples. http://www.mathworks.com/matlabcentral/fileexchange/12699

Carlson, M., 2019. org.Hs.eg.db: Genome wide annotation for Human. R package version 3.8.2

Cross Flow Filtration Method Handbook, 29-0850-76 AB 03/2014 a1675, GE Healthcare

Faisst, H. and Eckhardt, B. (2004). Sensitive dependence on initial conditions in transition to turbulence in pipe flow. Journal of Fluid Mechanics 504, 343-352.

Liberzon A., 2014. A description of the Molecular Signatures Database (MSigDB) Web site. Methods Mol Biol. 1150:153-160. doi:10.1007/978-1-4939-0512-6_9

Love, M.I., Huber, W. and Anders, S., 2014. Moderated estimation of fold change and dispersion for RNA-seq data with DESeq2. Genome Biol. 15(12):550. PMID: 25516281, PMCID: PMC4302049

Schramm, G., Wiesberg, S., Diessl, N., Kranz, A.L., Sagulenko, V., Oswald, M., Reinelt, G., Westermann, F., Eils, R., König, R., 2010. PathWave: discovering patterns of differentially regulated enzymes in metabolic pathways. Bioinformatics. 1;26(9):1225-31. doi: 10.1093/bioinformatics/btq113. PMID: 20335275

Selection Handbook, Hollow fiber cartridges and systems for membrane separations, 18-1165-29 AC, GE Healthcare

Shannon, P., Markiel, A., Ozier, O., Baliga, N.S., Wang, J.T., Ramage, D., Amin, N., Schwikowski, B., Ideker, T., 2003. Cytoscape: a software environment for integrated models of biomolecular interaction networks. Genome Res. 13(11):2498-504. PMID: 14597658, PMCID: PMC403769

Soneson C., Love. M.I., Robinson, M.D. Differential analyses for RNA-seq: transcript-level estimates improve gene-level inferences. *F1000Res*. 2015;4:1521. doi:10.12688/ f1000research. 7563.2

Väremo, L., Nielsen, J., Nookaew, I., 2013. Enriching the gene set analysis of genome-wide data by incorporating directionality of gene expression and combining statistical hypotheses and methods. Nucleic acids research 41(8): 4378-4391